



Cite this: DOI: 10.1039/c4dt02966f

A contribution to the rational design of Ru(CO)₃Cl₂L complexes for *in vivo* delivery of CO†

João D. Seixas,^{a,b} Marino F. A. Santos,^c Abhik Mukhopadhyay,^c Ana C. Coelho,^a Patrícia M. Reis,^a Luís F. Veiros,^d Ana R. Marques,^b Nuno Penacho,^b Ana M. L. Gonçalves,^b Maria J. Romão,^c Gonçalo J. L. Bernardes,^{‡,b} Teresa Santos-Silva^{*c} and Carlos C. Romão^{*a,b}

A few ruthenium based metal carbonyl complexes, *e.g.* CORM-2 and CORM-3, have therapeutic activity attributed to their ability to deliver CO to biological targets. In this work, a series of related complexes with the formula [Ru(CO)₃Cl₂L] (L = DMSO (**3**), L-H₃CSO(CH₂)₂CH(NH₂)CO₂H (**6a**); D,L-H₃CSO(CH₂)₂CH(NH₂)CO₂H (**6b**); 3-NC₅H₄(CH₂)₂SO₃Na (**7**); 4-NC₅H₄(CH₂)₂SO₃Na (**8**); PTA (**9**); DAPTA (**10**); H₃CSO(CH₂)₂CH(OH)CO₂H (**11**); CNCMe₂CO₂Me (**12**); CNCMeEtCO₂Me (**13**); CN(c-C₃H₄)CO₂Et (**14**)) were designed, synthesized and studied. The effects of L on their stability, CO release profile, cytotoxicity and anti-inflammatory properties are described. The stability in aqueous solution depends on the nature of L as shown using HPLC and LC-MS studies. The isocyanide derivatives are the least stable complexes, and the S-bound methionine oxide derivative is the more stable one. The complexes do not release CO gas to the headspace, but release CO₂ instead. X-ray diffraction of crystals of the model protein Hen Egg White Lysozyme soaked with **6b** (4UWN) and **8** (4UWV) shows the addition of Ru^{II}(CO)(H₂O)₄ at the His15 binding site. Soakings with **7** (4UWU) produced the metallacarboxylate [Ru(COOH)(CO)(H₂O)₃]⁺ bound to the His15 site. The aqueous chemistry of these complexes is governed by the water–gas shift reaction initiated with the nucleophilic attack of HO[−] on coordinated CO. DFT calculations show this addition to be essentially barrierless. The complexes have low cytotoxicity and low hemolytic indices. Following *i.v.* administration of CORM-3, the *in vivo* bio-distribution of CO differs from that obtained with CO inhalation or with heme oxygenase stimulation. A mechanism for CO transport and delivery from these complexes is proposed.

Received 26th September 2014,

Accepted 12th November 2014

DOI: 10.1039/c4dt02966f

www.rsc.org/dalton

Introduction

The biological role of CO as a signaling molecule¹ rapidly opened the way to the discovery of its biological applications. The cytoprotective, anti-inflammatory, anti-proliferative and anti-apoptotic properties of CO suggested its therapeutic use. Soon after the seminal report on the successful use of CO gas in a rodent model of LPS induced sepsis,² the concept of prodrugs capable of delivering CO, circumventing the shortcomings of CO gas inhalation, appeared in the patent literature.^{3–5} Among these, the derivatives of the fragment [Ru^{II}(CO)₃] introduced by Motterlini, Mann and co-workers first illustrated the use of metal-based CO-releasing molecules (CORMs) and became the golden standard in this novel therapeutic area.^{6,7} In fact, over 200 papers have been published in the last 10 years on the biological and therapeutic use of the two cornerstones of this family: [Ru(CO)₃Cl₂]₂ (CORM-2) and its water soluble glycinate derivative *fac*-[Ru(CO)₃Cl(κ²-H₂NCH₂CO₂)] (CORM-3).⁸ In spite of a recent contradictory report,⁹ these CORMs seem to have a low toxicity and produce

^aInstituto de Tecnologia Química e Biológica-António Xavier da Universidade Nova de Lisboa, Av. da República, EAN, 2780-157 Oeiras, Portugal.

E-mail: ccr@itqb.unl.pt; Tel: +351 214 469 751

^bAlfama Ltd., Instituto de Biologia Experimental e Tecnológica, IBET, Av. da República, EAN, 2780-157 Oeiras, Portugal

^cUCIBIO@REQUIMTE, Departamento de Química, Faculdade de Ciências e Tecnologia, Universidade Nova de Lisboa, 2829-516 Caparica, Portugal.

E-mail: tsss@fct.unl.pt; Tel: +351 212 948 300 (10940)

^dCentro de Química Estrutural, Instituto Superior Técnico, Universidade de Lisboa, Av. Rovisco Pais, 1049 Lisboa, Portugal

† Electronic supplementary information (ESI) available: FTIR spectra and HPLC traces for metal complexes. ¹³C NMR spectra of CORM-2 in DMSO solution. ESI-MS spectra for selected LC-MS fractions. Atomic coordinates for all DFT optimized species. See DOI: 10.1039/c4dt02966f

‡ Present address: Department of Chemistry, University of Cambridge, Lensfield Road, Cambridge CB2 1EW, UK and Instituto de Medicina Molecular, Faculdade de Medicina da Universidade de Lisboa, Av. Prof. Egas Moniz, 1649-028 Lisboa, Portugal.

a variety of beneficial therapeutic effects while keeping the values of carboxyhemoglobin (COHb) in circulation close to baseline values ($\leq 5\%$ COHb). Some remarkable examples of this therapeutic efficacy are given by CORM-3 in the protection against myocardial infarct and heart failure^{10,11} and the conservation of tissues for transplantation¹² and by CORM-2 in the protection of allogeneic aortic transplants in mice,¹³ but many other results can be found in several reviews.^{8,14,15}

This capacity to act in all these different organs and tissues at similar concentrations is somewhat surprising, and several questions regarding its mode of action are still unanswered. In fact, recent studies indicate that the mode of action of CORM-2 goes beyond its CO releasing activity, due to non-specific hydrophobic interactions¹⁶ or other biologically significant side-effects, e.g. ROS production.¹⁷

Until 2014, the derivatives of the $[\text{Ru}^{\text{II}}(\text{CO})_3]$ fragment studied under the perspective of their biological activity were limited to the methyl β -D-thiogalactoside (Gal-S-Me), the derivative *fac*- $[\text{Ru}(\text{CO})_3\text{Cl}_2(\text{Gal-S-Me})]$ (ALF492),¹⁸ the thiazole derivative $[\text{Ru}(\text{CO})_3\text{Cl}_2(\text{thiazole})]$ ^{19–21} and some analogues of CORM-3 bearing other amino acid ligands.⁴ ALF492 is much more efficient than CORM-3 in rescuing mice in a model of cerebral malaria without decreasing parasitemia, and this enhanced activity has been linked to selective accumulation in the liver. Indeed, it is reasonable to expect that the biological activity of the $[\text{Ru}(\text{CO})_3\text{Cl}_2\text{L}]$ complexes can be modulated by the nature of the ancillary ligand L. Understanding the nature of modulation for a given metal–carbonyl core is very important for the design of drug-like CORMs, as we have discussed elsewhere.^{22,23} ADMET (Absorption, Distribution, Metabolism, Excretion and Toxicity) and CO-release properties of a given CORM are both directly influenced by their inner and outer coordination spheres. The CO delivery mechanism of CORM-2 and CORM-3, once labeled “fast CO releasers”,²⁴ remains elusive, now that it has been proven that they are unable to transfer CO to deoxyMb as previously accepted.²⁵ The last observation is in agreement with the absence of CO in the headspace of solutions of CORM-3 or $[\text{Ru}(\text{CO})_3\text{Cl}_2(\text{thiazole})]$, as ascertained using highly sensitive GC methods.^{21,26} Besides the biodistribution study of ALF492, the only other ADME related observations made in the $[\text{Ru}^{\text{II}}(\text{CO})_3]$ based CORM literature were the rapid reaction of CORM-3 and $[\text{Ru}(\text{CO})_3\text{Cl}_2(\text{thiazole})]$ with proteins (e.g., lysozyme, serum albumin and transferrin) without CO release^{21,26,27} and the complex pH dependent speciation of these same complexes in aqueous biologically compatible media. However, during the writing of the present article a collection of fifteen $\text{Ru}^{\text{II}}(\text{CO})_3$ based CORMs with different ligands such as amino acid esters, amino-acidates, acetylacetonate, and pyridine derived ligands had their ADMET properties extensively examined.²⁸ The influence of the ancillary ligands on some of the properties of the complexes, including cell and *in vivo* toxicity, tissue absorption (Ru contents) and Ru biodistribution profile, is confirmed in the results reported. Moreover, this first study of the metabolism of this type of CORMs shows that Ru–CO complexes are absent in the urine and are generally poorly

retained in the main organs. The authors also confirm the reaction of these CORMs with plasma proteins and that “every CORM has several forms in blood due to hydrolysis”.²⁸

From the existing data it is undeniable that: (i) CORM-2, CORM-3 and ALF492 are biologically active both *in vitro* and *in vivo*; (ii) this activity is compatible with that expected for CO and often validated with independent CO gas treatments;¹⁴ (iii) solutions of CORM-3 release CO_2 , not CO, and become biologically inactive upon aging;^{7,26} (iv) CO is detected in cells treated with CORM-3 by the CO specific, fluorescent organometallic probe, COP-1 (CO probe 1);²⁹ and (v) the metal scaffold may also play a physiologically significant role.^{16,17} These apparently contradictory findings show that our understanding of the chemistry of $[\text{Ru}^{\text{II}}(\text{CO})_3]$ derived complexes under biological conditions warrants a further study in order to enable the design of analogues equipped with drug-like properties. In this manuscript we present the synthesis of a series of new $[\text{Ru}(\text{CO})_3\text{Cl}_2\text{L}]$ complexes where the variation of the nature of L is intended to provide information on the influence of the inner coordination sphere on the solubility, stability, reactivity, CO release profile, cytotoxicity, anti-inflammatory activity and other pharmacologically relevant properties of the complexes. We screen the interaction of some of these CORMs with proteins and examine important mechanistic features of their CO release profiles using protein X-ray crystallography and LC-MS spectrometry. Structural and reactivity results are also rationalized using DFT (density functional theory) calculations. Finally we present a detailed study of the bio-distribution of CO delivered by CORM-3 in mice.

Results and discussion

Synthesis and characterization of $\text{Ru}(\text{CO})_3\text{Cl}_2\text{L}$ complexes

The synthesis of new complexes of the formula $[\text{Ru}(\text{CO})_3\text{Cl}_2\text{L}]$ involves the cleavage of the chloride bridges of the commercially available dimer $[\text{Ru}(\text{CO})_3\text{Cl}_2]_2$ (CORM-2) as depicted in eqn (1).³⁰



This cleavage is usually performed in solvents (Solv) such as DMSO, THF, acetone or MeOH, where solvated species of the formula $[\text{Ru}(\text{CO})_3\text{Cl}_2(\text{Solv})]$ react with different ligands (L) to generate the target complexes. Since the aim of this study is the modulation of the physical, chemical and biological properties of the derivatives of the $[\text{Ru}^{\text{II}}(\text{CO})_3]$ fragment, we selected a collection of ligands with C, N, O, P or S donor atoms covering a broad range of coordinative properties. Iso-cyanide ligands of the type $\text{CNCR}_2\text{COOR}'$ (compounds **12**, **13** and **14** in this study) are isoelectronic with CO and have been successfully used in other organometallic drugs, namely in the cationic Cardiolite ($[\text{CNCr}_2\text{CMe}_2\text{OMe}]_6^+\text{A}^-$)³¹ and the liver active CORM $[\text{Mo}(\text{CO})_3(\text{CNCMe}_2\text{CO}_2\text{H})_3]$ (ALF794).³² These are weaker π -acids and stronger σ -donors than CO. The water soluble phosphines PTA (1,3,5-triaza-7-phosphaadamantane) and DAPTA (diacetylPTA; 3,7-diacetyl-1,3,7-triaza-5-phos-

phabicyclo[3.3.1]nonane) continue this trend as they are still weaker π -acids than isocyanides (compounds **9** and **10** in this study).³³ The pyridine ligands can be considered to represent biologically meaningful N-heterocyclic ligands, with modest π -acidity. Their substitution patterns were chosen to impart solubility through the sulfonate functionality (compounds **7** and **8** in this study). The methionine oxide (compounds **6a** or **6b** in this study) was selected to improve the biocompatibility and aqueous solubility relative to the DMSO complexes that result from dissolving CORM-2 in DMSO for biological applications (see below). Finally, the thioether (compound **11** in this study) represents a type of biologically relevant ligand which is regarded as electronically flexible but is usually rather labile in classical organometallic substitution reactions.³⁴ A sugar based thioether was successfully used in ALF492.¹⁸ The only O ligand used is DMSO in compound **3** and in some of the isomers of **4** and **5** in the series of known DMSO derivatives $[\text{RuCl}_2(\text{CO})_x(\text{DMSO})_{4-x}]$ ($x = 1, 2, 3$).³⁵ The structures of the new complexes of type $[\text{Ru}(\text{CO})_3\text{Cl}_2\text{L}]$ (**1–14**) are depicted in Fig. 1, together with CORM-2 and CORM-3. The details of syntheses are given in the Experimental section.

Reaction times and solvents used depended on the solubility of the selected ligand. Whenever solubility permitted, acetone was the solvent of choice. In the case of complexes **8** and **9** MeOH was used to circumvent the low solubility of the

corresponding ligands in acetone. The isocyanide complexes were prepared in CHCl_3 since the ligands are strong nucleophiles and readily cleave the Ru–Cl–Ru bridges at room temperature. The pale yellow or white solid products were isolated in moderate (53–63%) to good (73–85%) yields and were fully characterized using NMR, FTIR and elemental analyses. It is however important to note that the tricarbonyl complexes are not amenable to purification by recrystallization due to their lability in solution. In fact, they were all characterized after precipitation from their mother liquors by filtration followed by washing and drying. In the case of sulphonate complexes **7** and **8** we were unable to obtain a correct analysis due to the presence of residual amounts of water or the solvent of crystallization, which could not be entirely removed under vacuum (see the Experimental section). Some properties of the complexes are given in Table 1.

Table 1 CO vibrations in FTIR, water solubility and equivalents of CO and CO_2 released by CORM-2, CORM-3 and the other complexes described in this work (Fig. 1)

Compound	ν_{CO} (KBr; cm^{-1})	Water solubility ^d (mg mL^{-1})	Equivalents of CO released ^d	Equivalents of CO_2 released ^d
CORM-2	2144(s)	5 ^c	Not detected	1.80
	2090(s)			
	2069(vs)			
CORM-3	2139(s)	>20	Not detected ^g	0.68 ^e
	2057(s)			
3	1981(w)	2	Not detected	0.71
	2134(s)			
4 ^b	2068(s)	<3	Not detected	Not detected
	2077(s)			
5 ^b	2020(s)	>5	Not detected	Not detected
	2001(vs)			
6a	2131(s)	2	Not detected	1.20
	2055(s)			
6b	2131(s)	2	Not detected	—
	2055(s)			
7	2137(s)	>5	Not detected	0.96
	2053(s)			
8	2137(s)	>5	Not detected	1.00
	2053(s)			
9	2134(w)	Ins	Not detected	0.28
	2060(s)			
10	1994(s)	>5	Not detected	0.19
	2135(w)			
11	2067(s)	>5 ^c	Not detected	0.40
	2001(s)			
12	2141(s)	Ins (dec)	Not detected ^{f,g}	0.98 ^f
	2077(s)			
13	2063(s)	Ins (dec)	Not detected ^{f,g}	0.85 ^f
	2145(s)			
14	2093(s)	Ins (dec)	Not detected ^{f,g}	0.21 ^f
	2058(s)			
	2149(vs)			
	2090(s)			
	2061(vs)			
	2144(s)			
	2093(s)			
	2072(s)			

^a In H_2O , rt, except where noted. ^b A mixture of isomers is used. ^c 10% DMSO– H_2O . ^d Headspace of a H_2O solution; GC–TCD; dark; rt; N_2 atmosphere; 24 h. ^e PBS 7.4. ^f 25 mM in acetone–PBS 7.4 after 5 h. ^g Trace amounts of CO were detected after 4 h using GC–RCP. Ins = insoluble; dec = decomposition.

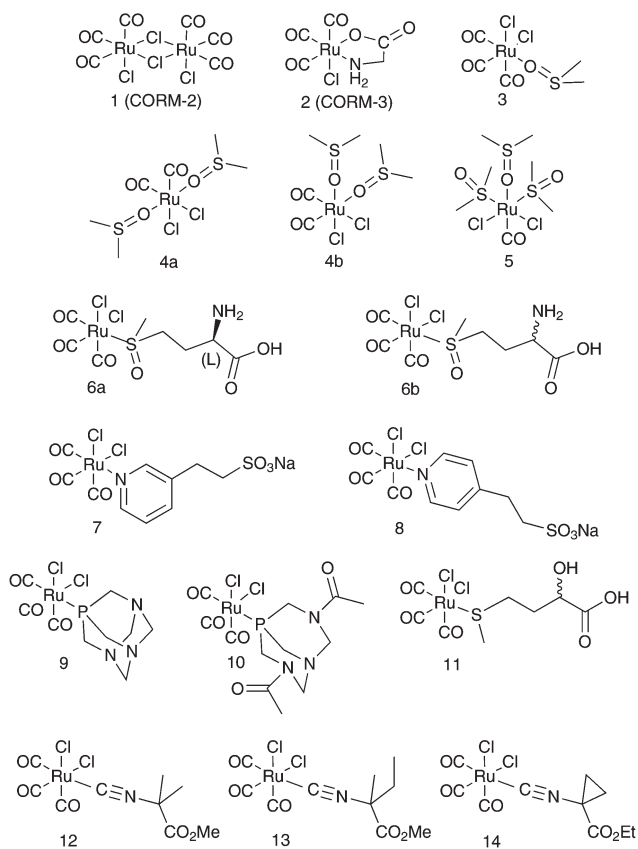


Fig. 1 Structures of CORM-2, CORM-3 and the new complexes described in this work.

The ^1H NMR spectra are very simple and show that the ligand protons shifted downfield due to the electron withdrawing character of the $\text{Ru}(\text{CO})_3\text{Cl}_2$ fragment. In the case of complexes **6a**, **b**, **7** and **8** the signals of the two CH_2 groups of the linear chain appear superimposed, affording one singlet in the ^1H NMR spectrum of each complex. The ^{31}P NMR spectra of the phosphine compounds **9** and **10** present chemical shifts in the range reported for other Ru complexes.^{33,36,37} In particular, the deshielding of the ^{31}P resonance of the DAPTA ligand, caused by coordination, is remarkable since it moves from δ (ppm) -78.5 in the free ligand to δ (ppm) 5.87 in **10**. The ^{13}C NMR spectrum of **12** shows at low fields two CO resonances (δ 183 and 182 ppm) and one CN resonance (δ 169 ppm), in agreement with a *fac*- $[\text{Ru}(\text{CO})_3\text{Cl}_2(\text{CNCMe}_2\text{CO}_2\text{Me})]$ configuration. The analogous complexes **13** and **14** have similar ^{13}C resonance values.

The FTIR spectra of most compounds present the usual ν_{CO} stretching band pattern corresponding to the *fac*- $\text{M}(\text{CO})_3$ fragment: a sharp, strong vibration at *ca.* 2135 cm^{-1} and a very strong, broader band at *ca.* 2055 cm^{-1} . The latter can be split as in compounds **9** and **10**, which show a weaker band at *ca.* 2135 cm^{-1} and a splitting of the lower wavenumber vibration in two strong bands at *ca.* 2060 cm^{-1} and 2000 cm^{-1} . This is probably due to the lowering of the local symmetry caused by the very bulky ligands. It is interesting to note the different coordination modes of the sulfoxide ligands in complexes **3** and **6a** (or **6b**) (see ESI S2 and S3† for details). While **3** shows a band at 903 cm^{-1} which is assigned to the ν_{SO} vibration of an oxygen bound Me_2SO ligand, both **6a** and **6b** have a band at 1017 cm^{-1} corresponding to a ν_{SO} vibration of a sulphur bound Me_2SO ligand in agreement with the versatility of the sulfoxide coordination chemistry.^{35,38} Those results are corroborated by DFT calculations (see DFT calculations) on complex **3**. The isomer with dimethylsulfoxide coordinated by the O-atom is 5 kcal mol^{-1} more stable than the isomer with S-coordinated sulfoxide, and the latter has a ν_{SO} vibration 230 cm^{-1} higher. The nature of the donor atoms (C, N, O, S or P) of the different ligands used does not cause major differences in the $\nu_{\text{C=O}}$ stretching vibrations of the corresponding complexes. Interestingly, the highest $\nu_{\text{C=O}}$ wavenumbers are found for the isocyanide complexes (*e.g.* **13** $\nu_{\text{C=O}}\text{ cm}^{-1}$: 2149, 2090, 2061) and the thioether complex in **11** ($\nu_{\text{C=O}}\text{ cm}^{-1}$: 2141, 2077, 2063). The $\nu_{\text{C=N}}$ vibration in the isocyanide complexes appears at *ca.* 2250 cm^{-1} .

Speciation of CORM-2 in DMSO

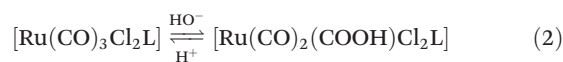
In all the cases reported so far, the addition of a ligand L to the $\text{Ru}(\text{CO})_3\text{Cl}_2$ core resulted in the octahedral complexes $[\text{Ru}(\text{CO})_3\text{Cl}_2\text{L}]$. However, some deviations from this pattern have been observed. In fact, the reaction of $[\text{Ru}(\text{CO})_3\text{Cl}_2]_2$ (CORM-2) with DMSO leads to complex **3** and the dicarbonyl complex *cis,trans,cis*- $\text{RuCl}_2(\text{DMSO})_2(\text{CO})_2$ (**4a**) as shown by ^{13}C NMR of a sample of CORM-2 measured over 29 min after dissolution in d^6 -DMSO.⁶ This spectral evolution is depicted in the ESI, Fig. S1.† Over a period of 18 h the tricarbonyl complex **3** is fully converted into the dicarbonyl isomers **4a** and the

more stable all *cis*-**4b**. The pure complex **3**, prepared independently,³⁵ when dissolved in d^6 -DMSO gives exactly the same dicarbonyl products with the liberation of CO gas (see Fig. S2 in ESI†). However, this CO loss does not progress beyond the dicarbonyl stage and after four days both isomers of **4** are still present in the ^1H NMR spectrum without formation of the monocarbonyl complex **5**. In fact, the dicarbonyl **4** and monocarbonyl **5** complexes are highly stable in the DMSO solution and no substitution of the carbonyl groups is observed at room temperature up to four days (NMR evidence not shown). The other peaks visible in the ^1H NMR spectrum correspond to the exchange of DMSO (or chloride) with residual H_2O present in d^6 -DMSO. A shift in the water resonance in the ^1H NMR spectrum can be detected over time (see Fig. S3 in ESI†). This easy exchange between DMSO and H_2O is similar to that described for $\text{RuCl}_2(\text{DMSO})_4$.^{39,40}

Solubility and stability in aqueous media

The solubility of the CORMs described above, in water or aqueous media compatible with their biological applications, was determined by visual inspection of solutions prepared with weighed amounts of the compounds in determined amounts of the solvent, at room temperature. A compound was considered soluble at a given concentration (mg mL^{-1}) if the solution obtained was visually clear and transparent. The tests were done at 1 mg mL^{-1} intervals. Since values above 5 mg mL^{-1} are usually appropriate to provide biologically and therapeutically useful working concentrations no higher solubility limits were determined except for CORM-3 as seen in Table 1. As expected, the majority of CORMs prepared are also quite soluble in water due to the nature of the ancillary ligands coordinated to the metal. In spite of being used to improve the water solubility of metal complexes in biological applications,⁴¹ the phosphine PTA is not able to guarantee the water solubility of **9**, which is completely insoluble. In contrast, the diacetylated version of PTA, DAPTA,³³ imparts a satisfactory solubility to $[\text{Ru}(\text{CO})_3\text{Cl}_2(\text{DAPTA})]$ (**10**). The isocyanide-derived complexes **12**, **13** and **14** are only slightly soluble in water where they readily decompose, darkening to an orange-brown color and releasing gas bubbles.

In contrast, the aqueous solutions of all other complexes remain clear and almost colorless, a fact that tells nothing about their stability. For instance, solutions of **7** and **8** in distilled water have a pH between 2.5 and 2.9, indicating that there is a reaction that increases $[\text{H}^+]$. This effect is similar to that discussed at length for *fac*- $[\text{Ru}(\text{OCOCF}_3)_2(\text{CO})_3(\text{H}_2\text{O})]$,⁴² CORM-3,⁴³ and $[\text{Ru}(\text{CO})_3\text{Cl}_2(\text{thiazole})]^{21}$ and is the result of the nucleophilic addition of HO^- to one of the CO ligands in the $[\text{Ru}^{\text{II}}(\text{CO})_3]$ fragment (see eqn (2)).



In order to further investigate the stability of the complexes in aqueous media, HPLC, LC-MS and ^1H NMR analyses were carried out for the following complexes: **3**, **4**, **6a** or **6b**, **10**. For

this purposes complexes **6a** and **6b** were considered equivalent species since **6b** is a mixture of **6a** and its optical isomer.

Aqueous solutions of the CORMs were prepared and aliquots eluted through a reverse phase HPLC column using the H₂O–MeOH gradient as described in the Experimental section and as shown in the ESI Fig. S4–S9.† A run was done every 15 minutes starting immediately after the dissolution of the compound ($t = 0$) and ending 60 min or 75 min later. None of the compounds tested can be considered stable in this time period since several peaks are present in the HPLC traces immediately after the dissolution. Some of these traces are shown in the ESI (Fig. S4–S9†).

The three DMSO derivatives **3**, **4** and **5** show a peak in the initial chromatogram ($t = 0$) with a retention time (RT) of *ca.* 7–9 min, which gradually disappears along time and which was assigned to the parent complex. Of the three, the more stable complex is the monocarbonyl **5**, which has a half-life of *ca.* 50 min and a 65% reduction 75 min after dissolution (Fig. S6 in ESI†). The dicarbonyl complex **4** decomposes rather quickly since the parent peak area (RT = 8.9 min) decreases 18-fold within the first 15 min post dissolution (see Fig. S5 in ESI†). These decay processes are certainly related to aquation reactions and do not produce any release of CO or CO₂ as described in the next section and Table 1. In the case of the tricarbonyl complex [Ru(CO)₃Cl₂(DMSO)] (**3**) the peak assigned to the parent complex (RT = 8.8 min) is already the third largest in terms of the Area Under the Curve measured in the initial ($t = 0$) chromatogram (Fig. 2 and Fig. S7 in ESI†). A peak with RT \approx 3.0 min increases along time for the three complexes. The HPLC chromatogram of CORM-2, dissolved in acetone, and eluted with the same MeOH–H₂O gradient actually consists essentially of a peak at RT = 3.0 min (Fig. S4 in ESI†). It is the most important one in all chromatograms of **3** but increases very little in the case of **4** and only appears at *ca.* 30 min post dissolution in the case of **5**. The remarkable biological activity of CORM-2 and its close relationship to complex **3** prompted our attempted identification of the dominant species in aqueous solutions of **3**. This was carried out using LC-MS analysis of a solution of **3** in 10% (v/v) methanol–water. The MS of the species observed at RT = 2.6 min has two large peaks at $m/z = 314.9$ and 392.5 which dominate over a large number of small signals spread up to $m/z = 1000$ (see Fig. S10

in ESI†). The $m/z = 392.5$ peak can be assigned to a species with the formulation [Ru(CO)₂(CO₂)(DMSO)₂Cl]⁺ (calcd $m/z = 392.88$). The more abundant peak at $m/z = 314.9$ corresponds to [Ru(CO)₂(CO₂)(DMSO)Cl]⁺ (calcd $m/z = 314.87$). These data are in agreement with the favorable attack of water on one of the CO ligands to generate a CO₂ ligand. The lability of the complex explains the easy exchange of chloride and DMSO ligands. This is also in agreement with the similar exchange observed by ¹H NMR with CORM-2 in DMSO solution (Fig. S3 in ESI†). No useful MS was obtained in negative ion mode.

The complex **6a** (or **6b**) possesses a methionine oxide ligand and is therefore very similar to **3** except for the fact that it is coordinated through the S atom and not through the sulf-oxide oxygen. Interestingly, HPLC reveals that **6b** is significantly more stable than **3** in solution, as can be seen in Fig. 2 (more details in ESI†). In fact, the peak at RT = 3.0 min is already present in the chromatogram of **6b** taken at $t = 0$ but it only grows a little until 60 min. Accordingly, the peak assigned to the parent **6b** complex (RT = 10.2 min) only decreases slightly during 60 min. An LC-MS analysis was carried out for **6a** in order to characterize the products in solution, both in positive and negative ion modes.

The MS of the peak with the lower retention time (2.0–2.4 min) in positive ion mode is dominated by the peak corresponding to the free methionine oxide (Met-O) ($m/z = 166.0$) and a stronger signal at $m/z = 487.0$ (see the MS spectrum in ESI, Fig. S11†). This can be assigned to the cation [Ru(CO)₂(Met-O)₂]⁺ (calcd $m/z = 486.98$). These are clearly decomposition products or even eventual impurities of the initial sample. The immediate next elution fraction (RT = 2.6–3.2 min) shows three main signals at $m/z = 240.88$, 281.65, 298.67 (in decreasing order of intensity). These masses are smaller than those of [Ru(CO)₂(Met-O)]⁺ ($m/z = 321.93$) and must correspond to smaller decomposition fragments. The peak at $m/z = 349.87$ found in the fraction with RT = 6.1–6.5 min can be assigned to [Ru(CO)₃(Met-O)Cl₂]⁺-2Cl ($m/z = 349.93$). Another strong peak at $m/z = 730.72$ seems to correspond to polynuclear decomposition products that aggregate more than one Ru ion. The positive ion mode ESI-MS spectrum of the fraction that carries **6a** (RT = 10.1–10.7 min) does not contain the parent ion peak. The LC-MS analysis carried out in negative ion mode presents one signal at $m/z = 384.8$ in the fraction with RT = 2.7–3.1 min (the fraction that increases along time), which can be tentatively formulated as [Ru-(COOH)(CO)₂{SO(CH₃)CH₂CH₂CH(NH₂)CO₂}(OH₂)]⁻ (calc. $m/z = 384.94$) (see Fig. S12 in ESI†). Importantly, a peak assignable to the parent anion [RuCl₂(CO)₃{SO(CH₃)CH₂CH₂CH(NH₂)CO₂}]⁻ (calc. $m/z = 421.86$) is found at $m/z = 421.7$ in the fraction with RT = 9.9–10.9 min, the fraction that slowly decreases along time in HPLC (see Fig. S13 in ESI†). The higher stability of **6a**, relative to **3**, is therefore corroborated by both the slow decay of its HPLC peak and the detection of its parent anion using ESI-MS. Finally, a peak at $m/z = 549.7$ found in the same elution fraction (RT = 9.9–10.9 min) can be assigned to the ion [RuCl(CO)₃{SO(CH₃)CH₂CH₂CH(NH₂)CO₂}]⁻ (calcd $m/z = 549.94$), a plausible decomposition product of **6a**. Somewhat

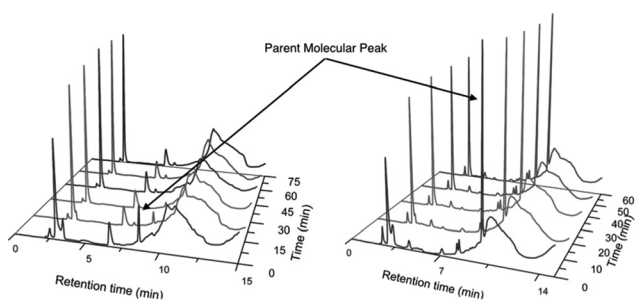


Fig. 2 HPLC traces of **3** (left) and **6b** (right) along time. Initial concentration: 1 mg mL⁻¹ in 10% DMSO–H₂O. Column: Nucleosil C18 (5 μ m) 150 mm \times 4.6 mm. Elution gradient: 10% MeOH–H₂O; flow: 1 mL min⁻¹.

unexpectedly, the phosphine derivative **10** proved relatively unstable and its HPLC trace shows many signals some of which increase in the region of RT = 2.5–3.0 min while other peaks decrease steadily (see ESI, Fig. S9†).

A brief survey of the stability of several of these complexes by ¹H NMR revealed the formation of species containing Ru–H bonds, which were detected after 24 hours in D₂O for **3** (δ –13.97 ppm), **6a** (δ –13.96 ppm), **7** (δ –13.94 ppm), and **8** (δ –13.94 ppm). These hydrides are similar to the one already identified before in aqueous solutions of CORM-3 (δ –14.5 ppm).²⁶ The formation of these hydride complexes is accompanied by the formation of CO₂ as will be shown in the next two sections.

CO and CO₂ release to the headspace in aqueous media

The rate of CO release from the compounds to the headspace of their solutions was evaluated in PBS7.4 or H₂O, at room temperature, in the dark, using gas chromatography (GC) with a TCD detector (see the Experimental section for details). Under these conditions none of the tricarbonyl complexes released CO to the headspace of their solutions (*ca.* 10 mg of the compound in 2 mL of medium, see Table 1). Only the use of the very sensitive GC-RCP chromatography enabled the detection of traces of CO after 4 h in solution. Instead, all complexes with [Ru(CO)₃] fragments produced CO₂. After 24 h the amount of CO₂ detected was found to vary with the nature of the ancillary ligands. It was smaller for the phosphine derivatives **9**, **10** (\approx 0.2 equiv.) and increased through the thioether **11** (\approx 0.4 equiv.) and CORM-2 (\approx 0.7 equiv.) to reach values of 1 equiv. and higher for the pyridine **7**, **8** and methionine oxide **6a**, **6b** derivatives. Two of the isocyanide complexes **12** and **13** released close to 1 equiv. CO₂ after 5 h in a solution of acetone–PBS (Table 1). The di-carbonyl complex RuCl₂(CO)₂(DMSO)₂ (**4**) and the mono-carbonyl RuCl₂(CO)(DMSO)₃ (**5**) do not release CO or CO₂ to the headspace of their solutions in PBS or H₂O at room temperature, in the dark, according to GC-TCD detection methods.

Interactions with proteins

The interaction between CORM-3 and a number of proteins has been previously described. These studies include Human Serum Albumin (HSA), human Transferrin (h-Tf), hemoglobin (Hb), myoglobin (Mb) and Hen Egg White Lysozyme (HEWL).^{26,27} Using single crystal X-ray diffraction, the 3D crystal structures of the model protein HEWL bound to CORM-3 and [Ru(CO)₃Cl₂(thiazole)] have been determined.^{21,26} In the present study we applied the same methodology to complexes **6b**, **7** and **8** in order to understand the mode of interaction of these newly synthesized CORMs with HEWL. Other complexes did not produce useful X-ray diffraction data.

Crystals of HEWL previously soaked with complexes **6b**, **7** and **8** were measured and complete data sets were collected at high resolution (see Table 2).

The structures were solved by MR using the native protein as the reference model (PDB code 193L⁴⁴) and refined with all residues in the allowed regions of the Ramachandran plot (see

Table 2 for refinement statistics). As expected the obtained models are highly similar to each other and to the native protein.

Common to the three structures is the presence of Ru species bound to His15 in an octahedral geometry (Fig. 3), as observed for the previously published HEWL·CORM-3 complex models.^{21,26} More Ru ions are also found at the surface of the protein bound to aspartate residues, which in some cases bridge two metal ions (see Table 3). In the obtained structures, not all the Ru atoms and the ligand atoms are fully occupied due to disorder at the ruthenium binding sites. Nevertheless, it is clear from the electron density that in the three CORM·protein complexes obtained, one or two of the initial CO ligands as well as the ancillary ligands are absent and have been replaced by water molecules.

In the crystal structures of the 7·HEWL complex, a less common electron density is observed in the coordination

Table 2 Data collection and refinement statistics for the organometallic-protein complexes formed between HEWL and **6b**, **7** and **8** (values in parentheses correspond to the highest resolution shell)

	6b ·HEWL	7 ·HEWL	8 ·HEWL
X-ray source	ID14-1 (ESRF)	ID14-2 (ESRF)	ID14-2 (ESRF)
Crystal data			
Space group	<i>P</i> 4 ₃ 2 ₁ 2	<i>P</i> 4 ₃ 2 ₁ 2	<i>P</i> 4 ₃ 2 ₁ 2
Unit cell parameters (Å, °)	<i>a</i> = <i>b</i> = 79.93, <i>c</i> = 36.89 α = β = γ = 90	<i>a</i> = <i>b</i> = 78.66, <i>c</i> = 37.00 α = β = γ = 90	<i>a</i> = <i>b</i> = 80.22, <i>c</i> = 37.16 α = β = γ = 90
Molecules per ASU	1	1	1
Mosaicity (°)	0.25	0.35	0.31
Matthews coefficient (Å ³ Da ⁻¹)	2.03	1.97	2.06
Solvent content (%)	39.50	37.71	40.37
Data collection			
Wavelength (Å)	0.933	0.933	0.933
Resolution range (Å)	30.89–1.67 (1.76–1.67)	27.81–1.78 (1.87–1.78)	28.36–1.77 (1.86–1.77)
<I/σI>	19.3 (5.1)	42.07 (19.6)	29.3 (10.3)
Multiplicity	7.0 (6.8)	13.8 (13.2)	13.8 (13.2)
Number of observed reflections	100 389 (14 122)	161 272 (21 868)	171 634 (23 241)
Number of unique reflections	14 435 (2064)	11 707 (1655)	12 432 (1757)
R _{pim} (%)	2.2 (14.8)	1.4 (4.4)	1.6 (6.3)
Completeness (%)	99.9 (100)	100.0 (100.0)	100.0 (99.9)
Refinement statistics			
Resolution range (Å)	30.89–1.67	27.81–1.78	28.36–1.77
R _{work} (%)	16.57	16.13	18.30
R _{free} (%)	21.15	19.52	22.20
RMSD bond length (Å)	0.013	0.010	0.019
RMSD bond angle (°)	1.53	1.29	1.81
Ramachandran plot (%)			
Residues in favored regions	96.06	96.06	95.28
Residues in additionally allowed regions	3.94	3.94	4.72
Residues in disallowed regions	0	0	0
PDB code	4UWN	4UWU	4UWV

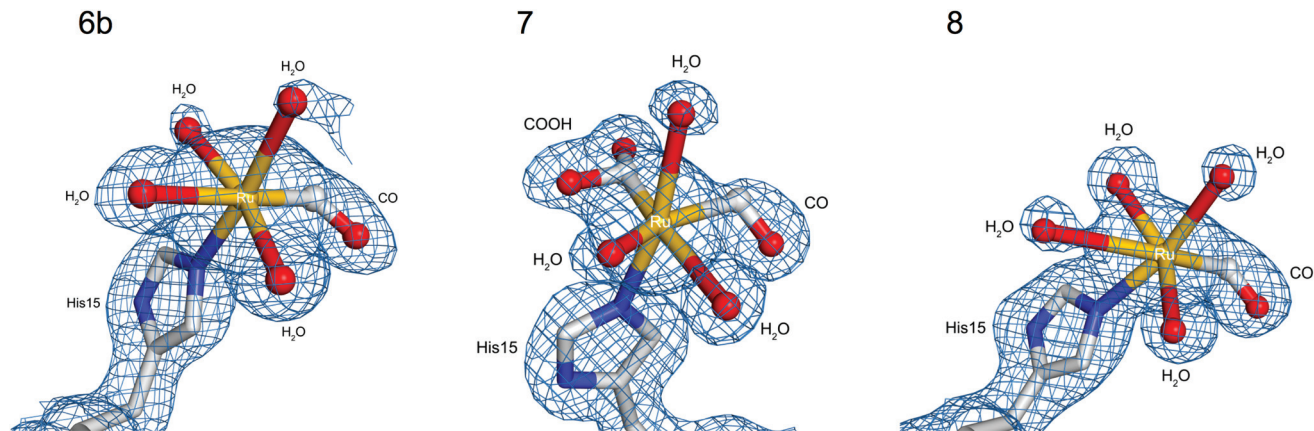


Fig. 3 Structural representation of the CORM·HEWL complexes at the site with the highest Ru occupation, obtained by soaking HEWL crystals with **6b**, **7** and **8**. Representation of the experimentally observed electronic density for each protein complex at the His15 site [map contoured at $0.3927 \text{ e } \text{Å}^{-3}$ (rmsd: 1), $0.4562 \text{ e } \text{Å}^{-3}$ (rmsd: 1) and $0.4003 \text{ e } \text{Å}^{-3}$ (rmsd: 1) for complexes **6b**, **7** and **8**, respectively]. The three CORM·HEWL complexes present an octahedral geometry at the Ru atom: in addition to the histidine residue (His15), the metal coordination sphere is completed with CO, COOH and H_2O molecules depending on the compound the HEWL crystals were treated with.

sphere of Ru at the His15 binding site. This electron density has been interpreted as a metallacarboxylate with a covalent Ru–C bond. Thus, the interaction of the tricarbonyl complex **7** with HEWL crystals led to the formation of a $[\text{Ru}(\text{CO})(\text{COOH})(\text{H}_2\text{O})_3]^+$ species, which is coordinated to the protein by the imidazole group of His15. Such a species is formed through the addition of HO^- to the dicationic fragment $[\text{Ru}(\text{CO})_2(\text{H}_2\text{O})_3]^+$.

DFT studies on structure and reactivity

The results described in the preceding sections, taken together with other studies previously reported,^{21,26,42,43,45} strongly suggest that the chemistry of the $[\text{Ru}(\text{CO})_3]^{2+}$ complexes in aqueous solution was initiated by the first step of the water-gas-shift reaction sequence, depicted in eqn (2). The initial tricarbonyl complexes add HO^- in a pH dependent equilibrium.

Table 3 Metal binding sites found in the crystal structures of HEWL soaked with **6b**, **7** and **8**, describing the ligands at each Ru binding site. Values in parentheses correspond to the occupancy of the ruthenium

CORM·HEWL adduct ligands	6b ·HEWL	7 ·HEWL	8 ·HEWL
His15 site	Ru (1) CO 4 H_2O	Ru (0.8) CO COOH ⁻ 3 H_2O	Ru (0.7) CO 4 H_2O
Asp18 site	Ru (0.65) CO 3 H_2O	Ru–Ru (0.5) 8 H_2O	
Asp52 site	Ru (0.5) 3 H_2O	Ru (0.4) CO 3 H_2O	
Asp101 site		Ru–Ru (0.7) Asp 101 6 H_2O	Ru–Ru (0.65) 5 H_2O
Asp119 site	Ru (0.5) 3 H_2O	Ru (0.7) CO 4 H_2O	

This equilibrium can only be pushed to the left at very low pH values and temperatures $\approx 0 \text{ }^\circ\text{C}$ as described for CORM-3⁴³ and for the extremely acidic *fac*- $[\text{Ru}(\text{CO})_3(\text{H}_2\text{O})_3]^{2+}$.^{42,45} When the pH rises above 3–4, HO^- addition pushes the equilibrium to the right and the metallacarboxylate species starts to appear. Inspection of the FTIR spectrum in the CO stretching region and the sudden pH variation registered upon dissolution in water indicate that the addition of HO^- to the $\text{Ru}(\text{CO})_3$ fragment of these compounds is highly favorable and fast. Accordingly, DFT modeling of the reaction of *fac*- $[\text{RuCl}_2(\text{CO})_3(\text{MeIm})]$ (MeIm = methylimidazole) with HO^- in the presence of H_2O (one molecule explicitly considered) revealed an extremely low kinetic barrier ($\Delta G^\ddagger = 0.4 \text{ kcal mol}^{-1}$) and a rather large negative free energy balance for the reaction ($-30.8 \text{ kcal mol}^{-1}$) as depicted in Fig. 4. The mechanism occurs in a single step, with HO^- attacking the C-atom of one CO ligand and yielding a COOH^- ligand bonded to the metal in the final product. Other computational studies of this reaction for several metal carbonyl complexes also confirm this addition to be essentially barrierless.^{46–52}

This kinetic profile hints that HO^- addition must be much faster than halide displacement. This is confirmed in Fig. 5 where the putative substitution of chloride by hydroxide in the complex $[\text{RuCl}_2(\text{CO})_3(\text{MeIm})]$ is modeled using DFT calculations. The reaction occurs in two consecutive steps. First, there is release of one Cl^- ligand, from **C** to **D**, indicating a dissociative mechanism. In the second step, from **D** to **E**, OH^- binds the metal atom, occupying the coordination position created by the loss of the chloride ligand. The overall barrier obtained ($\Delta G^\ddagger = 19.3 \text{ kcal mol}^{-1}$, with respect to **A**) indicates that this substitution reaction is considerably less favorable than HO^- attack on coordinated CO.

The results above strongly suggest that aqueous chemistry of $\text{Ru}(\text{CO})_3\text{Cl}_2\text{L}$ complexes effectively takes place from $[\text{Ru}(\text{COOH})\text{Cl}_2(\text{CO})_2\text{L}]^-$ and species of this kind are the ones that actually interact with the proteins and other biological entities

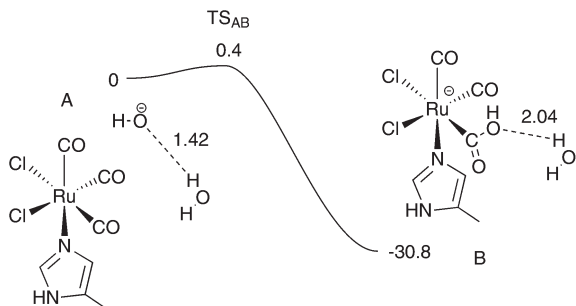


Fig. 4 DFT calculated free energy profile (kcal mol⁻¹) for the water assisted attack of HO⁻ on the model complex *fac*-[Ru(CO)₃Cl₂(MeIm)]. Bond lengths in Å.

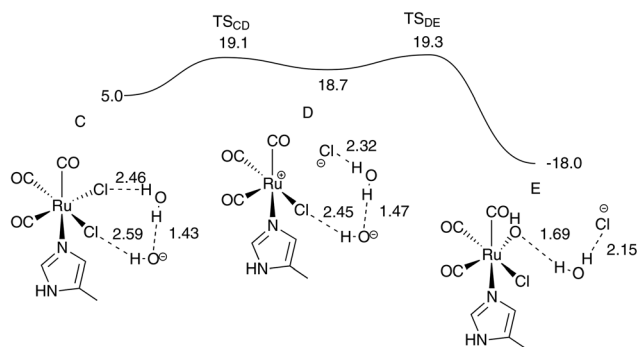


Fig. 5 DFT calculated free energy profile (kcal mol⁻¹) for the water assisted substitution of Cl⁻ by HO⁻ on the model complex *fac*-[Ru(CO)₃Cl₂(MeIm)]. Bond lengths in Å.

soon after incubation starts. Nevertheless, from the data gathered in this work, it seems that halides and other ligands L are easily displaced because they are absent in many of the peaks studied by LC-MS and are absent in all the organometallic-protein complexes identified using crystallography.

In the presence of proteins, the donor residues may substitute ligands from [Ru(COOH)Cl₂(CO)₂L]⁻ or may simply bind Ru fragments that are generated during its decay in solution without the participation of the protein. So far, and regarding only CO containing species, the data gathered from the interaction of HEWL with CORM-3,²⁶ [Ru(CO)₃Cl₂(thiazole)]²¹ and the above complexes **6b**, **7** and **8** led to the identification of the following [His15-Ru(CO)_x(H₂O)_yL] coordination motifs: [His15-Ru(CO)₂(H₂O)₃], [His15-Ru(CO)(H₂O)₄] and [His15-Ru(COOH)(CO)(H₂O)₃]. DFT calculations on similar Ru(II) complexes modeled with the methylimidazole ligand (MeIm) instead of the histidine yielded the results depicted graphically in Fig. 6.

According to these calculations, it is clear that the isomers identified in the protein crystal structures correspond to the thermodynamically most stable ones. The *fac*-[Ru(CO)₂(MeIm)(H₂O)₃]²⁺ isomer (**F**) is considerably more stable than the other *cis*-Ru(CO)₂ (**G**) and *trans*-Ru(CO)₂ (**H**) alternative isomers and corresponds to the isomer of the adduct [His15-Ru(CO)₂(H₂O)₃] present in the structure obtained from incubation of HEWL and CORM-3.²⁶ Also, the more stable isomer of the complex [Ru(CO)(MeIm)(H₂O)₄]²⁺ (**I**) places CO and

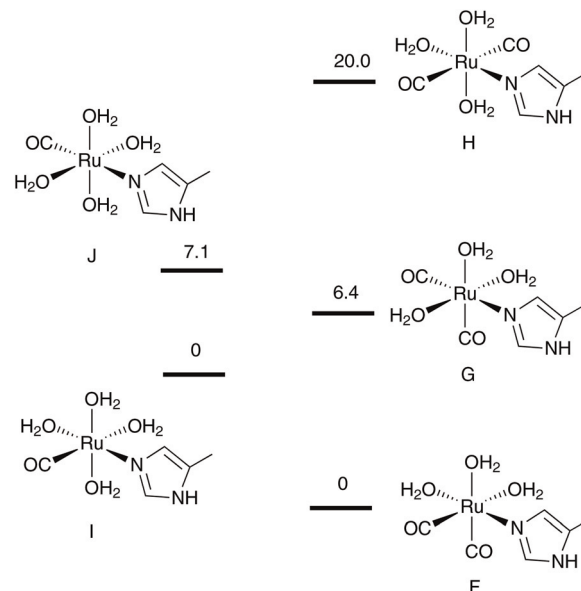


Fig. 6 DFT calculated relative energy differences (kcal mol⁻¹) between isomers of [Ru(CO)(H₂O)₄(MeIm)]²⁺ (**I**, **J**) and [Ru(CO)₂(H₂O)₃(MeIm)]²⁺ (**F**, **G**, **H**) where MeIm models the His15 ligand. The more stable isomers **F** and **I** have the same stereochemistry as that observed in similar CORM-HEWL complexes in Fig. 3.

MeIm at adjacent positions (*cis*), exactly as found in the cases of the organometallic-protein complexes obtained in the incubation of HEWL with [Ru(CO)₃Cl₂(thiazole)], **6b** and **8**.

In contrast to what happens with [Ru(CO)₃(H₂O)₃]²⁺, literature reports on the preparation and water exchange reactions of [Ru(CO)₂(H₂O)₄]²⁺ and [Ru(CO)(H₂O)₅]⁺ do not describe nucleophilic additions of water to CO in aqueous media. However, the *fac*-[His-Ru(COOH)(CO)(H₂O)₃]⁺ observed in the crystal structure of the HEWL crystals incubated with **7** corresponds to the structure expected for the addition of HO⁻ to the [His15-Ru(CO)₂(H₂O)₃]²⁺ complex. Loss of CO₂ from this adduct leads to [His15-Ru(CO)(H₂O)₄]²⁺, the more often observed mono-carbonyl motif at His15 and other binding sites of the CORM-HEWL complexes (see Table 3). It is important to take into account that the pH at which the soaking experiments took place (*ca.* 4.5) is much higher than the pH at which [Ru(CO)₂(H₂O)₄]²⁺ and [Ru(CO)(H₂O)₅]⁺ were prepared and studied.

Cytotoxicity studies

The cytotoxicity of the CORMs was measured using the concentration that causes an inhibition of 50% in the survival of cells upon incubation (IC₅₀). The results reported in Table 4 show that all the compounds investigated in this study were not toxic to RAW264.7 cells up to 100 μM. The isocyanide complexes were not tested due to their rapid decomposition in the presence of water.

Anti-inflammatory evaluation in vitro. All the CORMs tested in this study were able to decrease the NO production by LPS-stimulated RAW264.7 cells in a dose dependent manner (Table 4; Fig. S14 in ESI[†]). The most active compound in redu-

Table 4 Cytotoxicity of CORMs in RAW264.7 (MTT assay; 24 h incubation; IC₅₀) and their effect at 100 μM on the inhibition of NO production (% control) in LPS-induced RAW264.7 cells. Hemolytic index (%) at [CORM] = 1 mg mL⁻¹

CORM	IC ₅₀ (μM)	Nitrite (% control)	Hemolysis index (%)
CORM-3	>100	58	<10
CORM-2	>100	83	70 (0.5 mg mL ⁻¹)
3	>100	42	70 (0.5 mg mL ⁻¹)
6a	>100	52	10
7	>100	50	50
8	>100	40	50
9	>100	11	<10
10	>100	20	<10
11	>100	75	<10

cing NO production was the thioether derivative **11**, which was able to reduce nitrite levels in culture by 75% relative to control cells. This value is slightly lower than that found for CORM-2. However, it is important to note that CORM-2 has two times as many [Ru(CO)₃] fragments as all other shown CORMs at the same molar concentration. In accord, the NO inhibitory activity of **3** (42%), which is expected to be the major species in a fresh solution of CORM-2 in DMSO, has half the inhibitory activity registered for CORM-2 in these tests (83%). The other sulfoxide complex, **6a**, as well as the pyridine derivative **7** and CORM-3, are all stronger inhibitors of NO than **3**. The phosphine derivatives **9** and **10** were the least active compounds in this group.

Blood hemolysis. Before entering any *in vivo* studies, CORM candidates must be tested with regard to their hemolytic activity. The results of this test for some of the CORMs prepared are also given in Table 4. These show that the majority of the CORMs under study are much less hemolytic than CORM-2 or -3 which induce hemagglutination at 1 mg mL⁻¹ and are hemolytic at 0.25 mg mL⁻¹. In fact, only **7** and **8** showed a hemolytic index of 50% while the remaining tested CORMs present 10% or less hemolytic activity at 1 mg mL⁻¹ concentration.

CO bio-distribution after administration of CORM-3 *in vivo*. A successful CORM should be able to specifically deliver CO to tissues or organs under pathophysiological conditions. CO bio-distribution studies in mice after inhalation of air with 500 ppm CO for 30 min showed an increase in CO concentration in the kidney, heart, spleen, liver, lung and brain.⁵⁴ Given the wide use and promising results of CORM-3 in a variety of pre-clinical studies,¹⁴ we decided to evaluate the ability of CORM-3 to deliver CO specifically to organs and tissues and compare it with CO inhalation. The results are graphically expressed in Fig. 7 where the control is the concentration of endogenous CO present in untreated, healthy mice. Although our measurements do not distinguish between free, Hb-bound or Ru-bound CO, we can say that CO accumulates mainly in the liver, kidney and spleen. In fact, the accumulation in these organs increased by a factor of *ca.* 3, while that in the heart increases by a factor of 2 and the lungs and brain remain essentially at the base values. The accumulation in blood is not very important since the value of CO in the blood

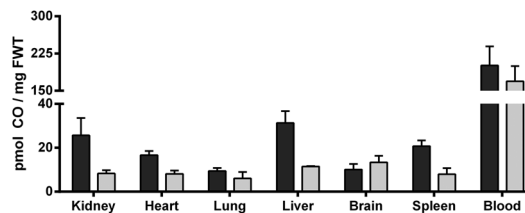


Fig. 7 CO levels in blood and tissues of CD-1 female mice treated with CORM-3, 50 mg kg⁻¹, iv (black bars), measured using GC-RCP. Control values for untreated, healthy CD-1 female mice are shown (grey bars). The GC-RCP results are expressed in pmol of CO per fresh weighed tissue (FWT) as means for two independent measurements. Animals were sacrificed 10 minutes after injection.

of the treated animals is only slightly more than that registered in the control animals. This is in agreement with the repeated observation that COHb levels in systemic circulation are barely affected by administration of CORM-3.^{10,55} Altogether, these data show that there is no apparent organ specificity in the bio-distribution of CORM-3. This is not unexpected given its simple and quite labile chemical structure. Of course, the modification of ancillary ligands can change this bio-distribution pattern giving it a higher bias towards specific target organs, as demonstrated in the case of the analogue [Ru(CO)₃Cl₂(methylthiogalactoside)] (ALF492) which shows a higher liver specificity albeit measured by the concentration of Ru instead of that of total CO.¹⁸ The bio-distribution in Fig. 7 differs considerably from that obtained with CO inhalation and reported by Vreman and coworkers.⁵⁴ Taking as 100% the blood concentration of CO generated by inhalation, Vreman and coworkers found that the CO concentrations in the other organs were *ca.* 1 or 2 orders of magnitude below the blood concentration (BC): lung (9.4% of BC), spleen (8.6% of BC), kidney (4.5% of BC), liver (4.3% of BC), heart (3.8% of BC) and brain (0.7% of BC). In the case of CO delivered by CORM-3 (Fig. 7), the accumulation in the other organs relative to blood is higher: liver (15.6% of BC), kidney (12.8% of BC), spleen (10.3% of BC), heart (8.3% of BC), brain (5.0% of BC) and lung (4.7% of BC). The stimulation of endogenous CO generation *via* heme oxygenase induction also gives the blood as the main CO loaded organ, followed by the heart and the spleen in an unspecific fashion.⁵⁴

These results indicate that CO delivery *in vivo*, *via* CORMs, originates a bio-distribution of CO which is clearly different from those obtained by endogenous CO production or CO inhalation. Considering that CORMs can be equipped with organ targeting features, it is obvious that they have a clear advantage over other methods of triggering CO protection. This has been argued before, but we believe that it is shown here quantitatively for the first time.

Conclusions

The undisputed activity of several Ru(CO)₃ complexes as prodrugs for the delivery of CO to biological systems *in vitro* and

in vivo contrasts with their lack of acceptable pharmacological properties and the limited understanding of their chemistry and mode of action. The present work represents an attempt to overcome this situation and contribute to the design of useful drug-like CORMs.

Acceptable solubility and stability in aqueous or biological media are forefront conditions to be met by a drug and CORMs are no exceptions. Such stability will enable the study of the pharmacokinetic behavior of the compound and ultimately its biological mode of action. However, as a prodrug, a CORM must also inscribe the chemistry that triggers its decomposition at the target organ, tissue, cell or biomolecule. This apparent contradiction can be solved by means of an appropriate combination of the inner and the outer coordination spheres of the organometallic CORM candidate.²² For a given organometallic core, the design pathway starts by establishing the inner coordination sphere that provides appropriate stability and reactivity control, as exemplified in the development of the liver rescuing $[\text{Mo}(\text{CO})_3(\text{CNCMe}_2\text{COOH})_3]$ (ALF794).³² The ADME and targeting profiling is carried out at a later stage through manipulation of the outer coordination sphere.

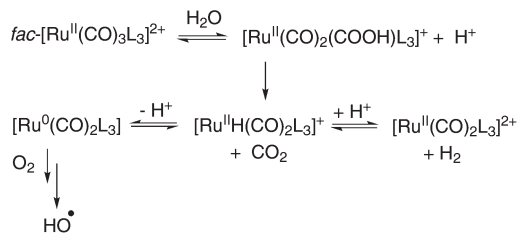
With these provisos in mind a series of complexes of the general formula *fac*- $[\text{Ru}^{\text{II}}(\text{CO})_3\text{Cl}_2\text{L}]$ was prepared with a broad range of donor functions L, namely *O*-sulfoxides, *S*-sulfoxides, pyridines, phosphines, thioethers and isocyanides (Fig. 1 and Table 1). The complexes are readily synthesized and characterized by standard procedures of organometallic chemistry. In spite of the different electronic abilities of the ligands used, the values of the $\nu_{\text{C}\equiv\text{O}}$ vibrations of the complexes (Table 1) do not vary widely except for the isocyanide (CNR) congeners, which are clearly more elevated. As the electronic properties of the $\text{Ru}(\text{CO})_3$ fragment remain essentially constant for most ligands the rest of the coordination sphere must accommodate the different electronic constraints imposed by the L ligands. The CNR ligands are strong enough σ donors and π acceptors to change this situation and reduce back-donation to the CO ligands.

Introducing sufficient water solubility by means of polar functionalization of the ligands was successful as can be seen in Table 1. The PTA complex **9** is a surprising exception. This ligand is considered a water-solubilizing phosphine^{37,41} but in this regard it is much less efficient than its DAPTA derivative in complex **10**. The isocynoacetate ester ligands were not expected to improve solubility *per se*, and indeed failed to do so. This lack of solubility was expected to be corrected at later stages by the use of their anionic forms CNCR_2COOM ($\text{M}^+ = \text{Li}^+, \text{Na}^+$).^{56,57} However, the instability of the CNR complexes in aqueous media discouraged such experiments.

The stability of the complexes in aqueous solution is rather more difficult to control than solubility. In fact, the extremely facile addition of HO^- to one of the CO ligands of the $\text{Ru}^{\text{II}}(\text{CO})_3$ fragment is certainly the main cause of instability and an intrinsic property of this scaffold (eqn (2)). As pointed out by DFT calculations made on the model complex $[\text{Ru}(\text{CO})_3\text{Cl}_2(\text{MeIm})]$, this addition has virtually no activation

barrier, in agreement with the fact that aqueous solutions of $[\text{Ru}^{\text{II}}(\text{CO})_3\text{L}_3]^{2\pm}$ compounds acquire a $\text{pH} \leq 3$ depending on the ancillary ligands. In other words, as pointed out by Mann and coworkers,⁴³ these complexes are able to react with HO^- at concentrations $\leq 10^{-11}$ M. Therefore, once dissolved in aqueous medium, the chemistry of the compounds $[\text{Ru}^{\text{II}}(\text{CO})_3\text{Cl}_2\text{L}]$ is governed by the reactivity of the metallacarboxylate species $[\text{Ru}^{\text{II}}(\text{CO})_2(\text{COOH})\text{Cl}_2\text{L}]^-$. Under biological conditions, with $\text{pH} \gg 3$, the equilibrium of eqn (2) is strongly driven to the right and the $\text{Ru}(\text{CO})_3$ fragment is completely absent in solution as shown by FTIR in the cases of CORM-3 and $\text{Ru}(\text{CO})_3\text{Cl}_2(\text{thiazole})$ solutions.²¹ It is under these conditions that it becomes important to ascertain the stability of the metallacarboxylate intermediate. If it is stable for a time span compatible with the time scale of the biological experiment, it is possible that it behaves as a stable prodrug with a recognizable and quantifiable pharmacokinetic profile. According to the HPLC tests performed with some selected complexes in $\text{MeOH-H}_2\text{O}$ the stability of the initially formed $[\text{Ru}(\text{CO})_2(\text{COOH})\text{Cl}_2\text{L}]^-$ complexes is very limited for most complexes studied, as exemplified in Fig. 2 and in the ESI, Fig. S4–S9.† Complex **3** or its HO^- adduct are tentatively assigned to a peak showing itself in the HPLC trace obtained immediately after dissolution in $\text{MeOH-H}_2\text{O}$ ($\text{RT} = 8.8$ min), but we could not obtain definitive proof of that using LC-MS with ESI detection. The closest peak identified that can be related to the metallacarboxylate derivative of **3** is $[\text{Ru}(\text{CO})_2(\text{CO}_2)(\text{DMSO})\text{Cl}]^+$ which appears in the highly water-soluble, first-eluting fraction of the chromatogram.

The case of CORM-2 is particularly interesting and worth discussing due to its extensive use in the literature. Our results show that according to the method of preparation of CORM-2 solutions for biological administration, **3** is the most abundant species in the DMSO stock solution of the dimer. Depending on the age of this stock solution, variable amounts of **4** are also present. When the solution is diluted in aqueous buffer at $\text{pH} 7.4$ for biological administration, both these species start immediate decomposition, making it impossible to assign the nature of the active biological species, the PK of the drug and the overall mechanism of action. The lipophilicity of both **3** and **4** may account for non-specific hydrophobic interactions observed with CORM-2, which operate beyond its CO delivery activity.¹⁶ Interestingly, the methionine oxide derivative **6a** or **6b** showed a much higher stability and the parent molecule and its HO^- adduct were found to be stable for 1 h along several consecutive HPLC runs in the same $\text{MeOH-H}_2\text{O}$ gradient as that used for **3**. The parent ion $[\text{RuCl}_2(\text{CO})_3(\text{SO}(\text{CH}_3)\text{CH}_2\text{CH}_2\text{CH}(\text{NH}_2)\text{CO}_2)]^-$ was identified using LC-MS in negative ion mode. This important result demonstrates that it is possible to generate an inner coordination sphere that stabilizes the $\text{Ru}(\text{CO})_3$ fragment or its HO^- adduct for a period of time compatible with biological testing. However, this is not yet easily predictable. The proverbial stability imparted by phosphine ligands to metal carbonyl complexes might have suggested improved properties for the PTA and DAPTA derivatives, which was not the case. Isocyanide derivatives became



Scheme 1 Reactivity of $[\text{Ru}^{\text{II}}(\text{CO})_3\text{L}_3]^{2+}$ CORMs in aqueous, aerobic solutions. All types of species presented have been identified for at least one such CORM.

intolerant to water due to excessive activation of CO. Surprisingly, sulfoxide and thioether ligands, which are considered very labile in classical organometallic chemistry, provided the best examples, eventually as a result of their extra functionalization.

Of course, when the metallacarboxylate species ages in solution it decomposes irreversibly, generating CO_2 , metal hydrides, hydroxyl radicals and other species that have been identified in this and previous studies. They can all be accommodated in the chemistry of Scheme 1.

In a typical water–gas-shift reaction (WGSR) pathway, the metallacarboxylate is initially formed, forming a *cis*- $\text{Ru}(\text{CO})_2$ moiety which is identified using FTIR spectroscopy and lowering the pH of the solution, as observed experimentally. This evolves to produce CO_2 and Ru–H complexes. Both CO_2 and Ru–hydrides were detected chromatographically and spectroscopically, respectively, confirming this reactivity pattern. According to the example reported by Fachinetti and co-workers, the complex $[\text{RuH}(\text{CO})_2(\text{H}_2\text{O})_3]^+$, which can be taken as a model for the Ru–hydrides derived from the complexes $[\text{Ru}(\text{CO})_3\text{Cl}_2\text{L}]$, can react with bases to lose H^+ and lead to the formal reduction of $\text{Ru}(\text{II}) \rightarrow \text{Ru}(\text{0})$.⁴² Such very electron rich $[\text{Ru}^{\text{0}}(\text{CO})_2\text{L}_3]$ complexes will react with O_2 to reform $\text{Ru}(\text{II})$ species and produce (HO^\bullet) radicals,^{58,59} which have also been observed experimentally using ESR spectroscopy in CORM-2 and CORM-3 aqueous aerobic solutions.^{17,60} Of course, one can also expect that such hydrides $[\text{RuH}(\text{CO})_2(\text{H}_2\text{O})_3]^+$ react with protons to produce H_2 . This was indeed detected in the case of CORM-3 aqueous solutions but not quantified.²⁶ Moreover, many $\text{Ru}(\text{CO})_3$ complexes, including CORM-2, are WGSR catalysts.⁶¹ The vibrational signature of the *cis*- $\text{Ru}(\text{CO})_2$ species that are formed by both modes of decomposition of the Ru–H intermediates is present in the FTIR spectrum of iCORM-3, the biologically inactive residue left after ageing CORM-3 solutions in aqueous buffer at pH 7.4 for 24 h in air. The fact that such iCORM solutions do not release CO may be due to either their strong stability or to the involvement of another addition of HO^- to those $\text{Ru}(\text{CO})_2$ species. Such addition was not reported for $[\text{Ru}(\text{CO})_2(\text{H}_2\text{O})_4]^{2+}$ since it was prepared and characterized in acidic medium, but has been well documented in this work (see Fig. 2) and with the dication *cis*- $[\text{Ru}(\text{bpy})_2(\text{CO})_2]^{2+}$. This reacts with HO^- to form first $[\text{Ru}(\text{bpy})_2(\text{CO})(\text{COOH})]^+$ and then $[\text{Ru}(\text{bpy})_2(\text{CO})(\text{CO}_2)]$ at higher pH, and behaves as a WGSR catalyst producing CO_2 and H_2 from CO and H_2O .^{62–64}

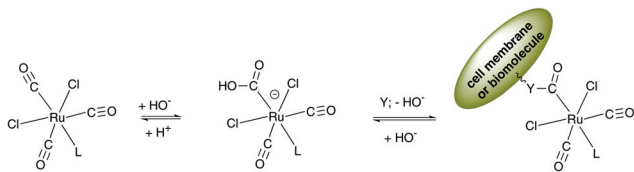
When this complicated chemistry takes place under biological conditions, two situations may happen: (i) it takes place independently of the biological species present, which may then react with the reaction/decomposition products; (ii) the presence of the biological molecules modulates the decomposition process.

Since this is crucial information for the study of the CO delivery mechanism of potential CORMs of the type $\text{Ru}(\text{CO})_3\text{Cl}_2\text{L}$ we studied the interaction of several of these compounds with the model protein Hen Egg White Lysozyme (HEWL).

The results obtained show that $\text{Ru}(\text{CO})_x$ fragments bind several residues of the HEWL protein (Table 3) but the adduct with His15 residue is the one that systematically presents the highest occupancy. As depicted in Fig. 3 both complexes **6b** and **8** generated the fragment $\text{Ru}^{\text{II}}(\text{CO})(\text{H}_2\text{O})_4$ bound to His15 as found in similar experiments with $\text{Ru}(\text{CO})_3\text{Cl}_2(\text{thiazole})$.²¹ The chloride ligands are absent in the final adduct, attesting their lability. The ultimate fate of the initial $\text{Ru}(\text{CO})_3\text{Cl}_2\text{L}$ complex is the loss of two CO ligands, the two Cl^- ligands and the ancillary ligand L: pyridine (**8**), methionine oxide (**6b**) or thiazole.

We have previously identified a *cis*- $\text{Ru}(\text{CO})_2(\text{H}_2\text{O})_3$ fragment bound to the His15 residue in similar experiments with CORM-3. In that case one CO and all other ligands were lost following the first addition of HO^- to the $\text{Ru}(\text{CO})_3$ fragment. Quite interestingly, the soaking of HEWL with **7** led to the identification of the metallacarboxylate intermediate $[\text{His15-Ru}^{\text{II}}(\text{COOH})(\text{CO})(\text{H}_2\text{O})_3]$ derived from the addition of HO^- to the dicarbonyl dication *cis*- $[\text{Ru}(\text{CO})_2(\text{H}_2\text{O})_3]^{2+}$. Crystallographic resolution does not allow distinguishing the metallacarboxylate from the corresponding $\text{Ru}(\eta^1\text{-CO}_2)$ species, but at pH 4.5 we favor the presence of the Ru–COOH fragment. Indeed, the stability and fate of this metallacarboxylate is pH dependent: higher pH will drive it to CO_2 and other Ru species, and lower pH will revert it to the parent dicarbonyl complex. It is now obvious that the use of HEWL has allowed us to capture a series of snapshots along the pathway of the decomposition of $[\text{Ru}(\text{CO})_3\text{Cl}_2\text{L}]$ complexes in aqueous medium, which is now very clear. The loss of the last CO has not been well documented here beyond some Ru ions bound to surface aspartates, but we believe that it can be easily modeled from the analogue $[\text{Ru}(\text{CO})(\text{H}_2\text{O})_5]^{2+}$. The wavenumber of the CO vibration in this complex (1971 cm^{-1}) suggests that it has a much lower electrophilicity at its Ru bound C atom than the $[\text{Ru}(\text{CO})_2(\text{H}_2\text{O})_4]^{2+}$ ($2089, 2023\text{ cm}^{-1}$) and $[\text{Ru}(\text{CO})_3(\text{H}_2\text{O})_3]^{2+}$ ($2170, 2084\text{ cm}^{-1}$) analogues, and the complex most likely decomposes by CO dissociation, which is likely to happen through the oxidation of $\text{Ru}(\text{II})$ to $\text{Ru}(\text{III})$.

The structures of all these $\text{Ru}(\text{CO})_x$ -HEWL complexes at the His15 binding site (Fig. 3) are those thermodynamically predicted by DFT calculations. It is not possible to ascertain the role (if any) of the protein in the decomposition of the $\text{Ru}(\text{CO})_3\text{Cl}_2\text{L}$ complexes and formation of the $\text{Ru}(\text{CO})_x$ -HEWL species. However, the reaction of CORM-3 with HEWL monitored using ESI-MS suggests that the protein actually accelerates



Scheme 2 The proposed mechanism for the interaction of $[\text{Ru}^{\text{II}}(\text{CO})_3\text{Cl}_2\text{L}]$ with cells or biomolecules.

ates the first loss of CO and other ligands leading to the exclusive formation of a $\text{Ru}(\text{CO})_2$ complex, $\text{Ru}(\text{CO})_2\cdot\text{HEWL}$, within a few minutes after incubation.²⁶

A relevant and often asked question still remains to be addressed: if these molecules are so labile and do not release CO gas to their biological environment, how do they deliver CO to cells and elicit CO dependent biological responses?

We believe that the chemistry described in Schemes 1 and 2 provides an easy general answer to this question.

If the metallacarboxylate lasts long enough in the biological medium, it gets to cells where it can exchange its added HO^- with any other ROH (transesterification) or RNH_2 (transamidation) terminal group present at the surface of the cells, thus anchoring the Ru complexes as adducts of the formula $[(\text{cell-Y-CO})\text{Ru}(\text{CO})_2\text{L}_3]$ and $[(\text{cell-Y})\text{Ru}(\text{CO})_2(\text{H}_2\text{O})_3]$ ($\text{Y} = \text{O}, \text{NH}$) at a later stage following CO_2 loss.

In this way, these CORMs can accumulate efficiently at the surface of cells and actually move from cell to cell by means of reversible exchanges with carrier molecules in the intercellular medium. This anchoring of the CORM to the cell surface enables decomposition or internalization of the Ru scaffold to take place at or inside the cell. In both cases CO will be readily available to the cell and its internal targets, e.g. mitochondria. In the case of internalization, the amount of CO delivered to the cell can be much higher than that usually achieved by dissolved free CO, which rapidly diffuses across membranes. This mechanism is compatible with the observations made with the CO sensitive fluorescent probe COP-1, showing that CORM-3 accumulates at the membrane and CO slowly builds up in the cytoplasm.²⁹

When these CORMs are administered *in vivo*, a $\text{Ru}(\text{CO})_2$ -albumin complex is likely responsible for the distribution and delivery of CO to other cells in the organism.²⁶ CORM-3 has produced *in vivo* curative results in diseases affecting quite different organs, such as joints, heart, arteries and others. This lack of selectivity is compatible with the $\text{Ru}(\text{CO})_2$ -albumin based distribution mechanism. The CO bio-distribution study in Fig. 7 reveals that all the organs studied have increased quantities of CO relative to the controls, with a higher incidence in liver and kidney. However, one cannot really talk about a specific accumulation in a given organ and CO from CORM-3 is smeared all over the organism. Importantly, this bio-distribution profile is different from that obtained by Vreman upon stimulation of endogenous heme oxygenase (HO).⁵⁴ This signals the therapeutic advantage of CORMs over HO since CORMs can direct CO to the organ of interest if prop-

erly targeted. Tissue targeting was not addressed in the present study but its efficacy has been demonstrated for $[\text{Ru}^{\text{II}}(\text{CO})_3\text{Cl}_2(\text{methylthiogalactoside})]$ (ALF492)¹⁸ and $[\text{Mo}(\text{CO})_3(\text{CNCMe}_2\text{COOH})_3]$ (ALF794).³² Of course, as pointed out by one of the referees, the very rich and complex chemistry of these $\text{Ru}^{\text{II}}(\text{CO})_3$ based CORMs, summarized in Scheme 1, may also contribute to some of their biological effects. The formation of ROS species downstream of the water-gas shift reaction may actually be relevant in some cases, since these species are strongly involved in signaling processes, including those involving CO. Some of these possibilities have been raised and discussed elsewhere,^{16,17,60} but the present data do not provide any evidence favoring or disfavoring them.

The complexes described in this study present an acceptably low cytotoxicity profile and the majority is not hemolytic. The classical test for anti-inflammatory activity, the NO inhibition of LPS-induced macrophages, does not reveal any extraordinary activity, but reveals some dependence on the nature of the ligand L. The thioether derivative **11** markedly inhibits the NO production of the LPS stimulated RAW264.7 macrophages by 74%. Interestingly, the value found for **3** is almost exactly one-half that found for CORM-2, in agreement with the latter forming 2 equivalents of **3** upon dissolution in DMSO.

Taken together, the data presented in this work contribute to the understanding of the chemistry and mode of action of different $\text{Ru}(\text{CO})_3\text{Cl}_2\text{L}$ complexes regarding stability, CO and CO_2 releasing profile and interaction with proteins. A set of different ligands with different chemical properties has been chosen for this systematic characterization. Reasonably stable and soluble complexes were obtained. Low cytotoxicity and considerable anti-inflammatory effects are found across all the complexes, showing that $\text{Ru}(\text{CO})_3$ based CORMs may have a future role in CO therapy.

Experimental section

General procedures

All work involving animals performed in the Lisbon laboratories of Alfama Ltd was done according to the guidelines of the Portuguese animal protection law and the derived guidelines on the ethical use of animals.

Gas chromatography with TCD detection

The CO release assays were performed in a 7.0 mL Roth® sample vial equipped with a magnetic stirrer inside and capped with a PTFE rubber or silicone septa and an aluminum cap. PTFE rubber septa were acquired from Sigma Aldrich® and a silicone septa from Roth®. The assays were performed in PBS7.4 or H_2O , without light, at room temperature and normal atmospheric air. For compounds **12**, **13** and **14** stock solutions were prepared in acetone, and then aliquots were added to PBS7.4, obtaining final solutions of 2 mL with concentrations of 25 mM for each compound. These were then placed in the Roth® vials as described above. 250 μL samples

of the headspace gas were taken with a gas tight Hamilton® syringe and were injected into a Thermofinnigan Trace GC equipped with a CTR1 column from Alltech™ and a Thermal Conductivity Detector. The column was in an oven at 36 °C and the GC was operated at a constant pressure mode (111 kPa) with He as a carrier gas and a reference gas with a 30 mL min⁻¹ flow rate. The detector was set at constant temperature (150 °C) and the filament temperature at 250 °C. The injections were made through a packed column injector (PKD) set at 47 °C and 111 kPa. CO was quantified using a calibration curve recorded prior to the reaction course. This was done by injecting 250 µL increments of CO up to a final total amount of 2 mL of pure CO gas (carbon monoxide 4.7, purity ≥99.997%; from Linde) into the system and taking samples that were injected in the GC.

Gas chromatography with RCP detection

Stock solutions of compounds **12**, **13** and **14** were prepared in acetone. 1 mL of the solution was added to 1 mL of PBS7.4 obtaining final solutions of 2 mL with concentrations of 25 µM for each compound. Each sample was prepared in triplicate. The final solutions were prepared and immediately closed in a 7.0 mL Roth® sample vial equipped with a magnetic stirrer inside and capped with a silicone/PTFE septa and an aluminum cap. Silicone/PTFE and an aluminum cap were acquired from VWR™. The vials were also immediately covered with aluminum foil to prevent contact with light and the solution was stirred at room temperature. Samples (100–200 µL) were taken from the headspace over time (5, 15, 30, 60, 120, 180 and 300 min), with a Gas tight Hamilton® syringe, and diluted in another 7.0 mL Roth® vial, capped with a silicone/PTFE septa and an aluminum cap, and analyzed quantitatively on a Peak Performer 1 RCP gas chromatograph (GC), which allows the CO in the gas to be quantified to concentrations as low as 1 to 2 ppb. The reducing compound photometer (RCP) bed and the column were set at constant temperatures, 265 and 105 °C, respectively.

The amount of CO was calculated using a calibration curve previously obtained in vials of the same volume (7.0 mL), using a Linde minican® of CO (30 ppm CO rest in synth. air), ref. 14960013.

X-ray crystallography

Hen Egg White Lysozyme (HEWL) has been used as a model protein for understanding the interaction between CORMs and proteins.

Crystals of HEWL have been prepared using NaCl (2–10% m/v) in acetate buffer (pH 4.5) as the precipitating agent. The crystals appear after 1–2 days with 0.2 × 0.2 × 0.2 mm³ dimensions. Soaking procedures have been performed as previously described,²⁶ dissolving the complexes of interest (**6b**, **7** and **8**) in a solution containing 12% m/v of NaCl in acetate buffer (pH 4.5) up to a final concentration of 50 mM. After 24 h of soaking, the crystals were harvested and flash frozen using 30% glycerol as a cryoprotectant. Complete data sets have been collected using synchrotron radiation and the crystals belong

to space group *P*₄₃₂₁² (see Table 2 for data collection statistics).

Structure determination was accomplished by molecular replacement using as a search model the structure with PDB code 193L, and several cycles of restrained refinement in Refmac⁵⁵ followed by manual model building in Coot⁶⁶ enabled us to produce the final models with a good geometry; PDB_REDO⁶⁷ was used for the validation of the final models (see Table 2 for refinement statistics).

The coordinates and structure factor have been deposited in PDB with accession numbers 4UWN, 4UWU and 4UWV (**6b**, **7** and **8**, respectively).

DFT calculations

All calculations were performed using the Gaussian 09 software package,⁶⁸ and the PBE0 functional, without symmetry constraints. That functional uses a hybrid generalized gradient approximation (GGA), including a 25% mixture of Hartree–Fock⁶⁹ exchange with DFT⁷⁰ exchange–correlation, given by the Perdew, Burke and Ernzerhof functional (PBE).^{71,72} The optimized geometries were obtained with the Stuttgart Effective Core Potentials and the associated basis set^{73–75} augmented with an f-polarization function⁷⁶ for Ru and a standard 6-31G (d,p)^{77–80} for the remaining elements. Solvent effects (water) were considered in optimizations of all species involved in the mechanistic studies, using the Polarizable Continuum Model (PCM) initially devised by Tomasi and coworkers^{81–84} with radii and non-electrostatic terms of the SMD solvation model, developed by Truhlar *et al.*⁸⁵ Transition state optimizations were performed with the Synchronous Transit-Guided Quasi-Newton Method (STQN) developed by Schlegel *et al.*,^{86,87} following extensive searches of the Potential Energy Surface. Frequency calculations were performed to confirm the nature of the stationary points, yielding one imaginary frequency for the transition states and none for the minima. Each transition state was further confirmed by following its vibrational mode downhill on both sides and obtaining the minima presented on the energy profile.

Cytotoxicity evaluation

The toxicity of the compounds was evaluated in a murine macrophage cell line RAW264.7 (ECACC91062702) using the MTT assay. Briefly, RAW264.7 cells were seeded on 96-well plates in DMEM medium (GIBCO, Invitrogen) supplemented with 10% FBS (Fetal Bovine Serum; GIBCO, Invitrogen). Cells were incubated for 24 hours at 37 °C, 5% CO₂ under a humidified atmosphere before the addition of the compounds to be tested. Compounds were solubilized in water or in 10% DMSO–H₂O (**3**, **9**, and **11**) and added to the macrophage cultures at a final concentration of 10, 50 or 100 µM. In the control wells, cells were treated with the solvent used to dissolve the compounds. The final DMSO concentration in cultures was never above 0.1%. Cells were incubated for 24 hours under the same conditions as those described above. The culture medium was replaced by a 1 mg mL⁻¹ of MTT solution prepared in DMEM-FBS supplemented medium and the cul-

tures were incubated for 1 hour at 37 °C, 5% CO₂. The supernatants were discarded and the formazan crystals produced were dissolved in DMSO. The plates were incubated with gentle shaking for 10 minutes and the absorbance of the medium was read at 550 nm. The absorbance obtained in the control wells was considered as 100% survival.

LPS stimulation of RAW264.7 cells and nitrite quantification

Murine macrophages RAW264.7 were seeded into the wells of a 24-well plate in DMEM medium supplemented with 10% FBS. Cells were incubated for 24 hours at 37 °C, 5% CO₂ under a humidified atmosphere. Compounds were added to the cultures at a final concentration of 10, 50 and 100 μM. At the same time lipopolysaccharide (LPS; L2880, Sigma) was added to the cultures at a concentration of 1 μg mL⁻¹. After 24 hours the NO production was determined by quantifying the nitrite in culture supernatants using the Griess reagent (Sigma). In a 96-well plate, 100 μL of the Griess reagent was mixed with the same volume of the culture supernatant and allowed to react for 10 minutes. The absorbance was read at 550 nm. A sodium nitrite standard reference curve was prepared for each assay for the accurate quantification of nitrite levels in experimental samples.

Hemolysis index determination

Red blood cells (RBC) obtained upon centrifugation of sheep whole blood (in Alsever's solution; Innovative Research cat. no. IR1-020N) were used to evaluate the potential of the Ru-complexes to induce RBC hemolysis. A 2% RBC suspension in PBS (100 μL) was distributed in the wells of a 96-well plate. The complexes were evaluated at concentrations between 0.0078 and 1 mg mL⁻¹. A 2 mg mL⁻¹ solution of the complexes in PBS (water solvent complexes) or in 10% DMSO + PBS (non-water solvent complexes) was prepared followed by 1:2 serial dilutions in the same solvent. These solutions were added (100 μL) to the RBC suspension. A 2% RBC solution in water was used as a positive control (RBC lysis). As the negative control, the 2% RBC suspension was also incubated with the solvents of each compound. The mixture of complex-RBC suspension was then incubated for 1 h at 37 °C.

The plate was then centrifuged and the absorbance of the supernatant was measured at 550 nm on a microplate reader (Bio-Rad). The hemolytic index (HI) was determined using the formula:

$$\text{HI}(\%) = \frac{\text{OD (complex sample)} - \text{OD (complex reference)}}{\text{OD (positive control)} - \text{OD (negative control)}} \times 100$$

where OD (complex reference) = OD of the corresponding complex solution (endogenous abs.). OD (positive control) = OD of the solution obtained by lysis of the RBC (1% RBC). OD (negative control) = OD of the 1% RBC suspension in the complexes' solvent after centrifugation.

A hemolytic index above 10% indicates hemolysis.

In vivo bio-distribution of CO

CD-1 female mice from Charles-River (6–8 weeks) were treated with 50 mg kg⁻¹ of CORM-3 (i.p.) in saline. After the respective times (10, 30 or 60 min) animals were sacrificed and perfused with 15 mL of PBS. Blood and livers were collected and diluted 50 times or 5 times, respectively, in ice-cold Milli-Q water (liver tissue was homogenized using a Tissue Tearor™). For CO quantification, the protocol described by Vreman *et al.* was followed.⁵⁴ Briefly, CO was liberated as a gas in a closed vial by adding 25 μL of water and 5 μL of sulfosalicylic acid (SSA, 30% [wt/vol]) to 30 μL of diluted samples. The vials were incubated on ice for at least 10 min before being analyzed. The gas in the headspace of the vials was analyzed quantitatively with a gas chromatograph (GC) equipped with a reducing-compound photometry detector (RCP detector) (Peak Laboratories, Mountain View, CA), which allows to quantify CO in the gas at concentrations as low as 1–2 parts per billion (ppb). The amount of CO was calculated using a calibration curve prepared from CO standards. Control animals were injected with a vehicle and handled in the same way.

Chemical synthesis

All preparations were performed under an atmosphere of nitrogen using standard Schlenk techniques. Solvents were dried by standard procedures, distilled under nitrogen and kept over 4 Å molecular sieves, except for DMSO that was used as received (*p.a.* from Panreac). Microanalyses for CHN were performed at the ITQB, Oeiras, Portugal (by C. Almeida). ¹H and ¹³C NMR spectra were recorded on a Bruker Avance III 400 MHz. Chemical shifts are quoted in parts per million. FT-infrared spectra (KBr pellets) were recorded in a Unicam Mattson 7000 FTIR spectrophotometer. ATR-FTIR (Attenuated Total Reflection Fourier Transform Infrared) spectra in solution (MeOH and PBS) were recorded in a Bruker IFS66/S spectrometer at room temperature. Ru(DMSO)₄Cl₂ and [Ru(CO)₃Cl₂]₂ were purchased from Strem Chemicals. L-Methionine sulfoxide and 2-hydroxy-4-(methylthio)butyric acid calcium salt were purchased from Fluka. Pyridine-based ligands were purchased from Asis Chem. Inc. 1,3,5-Triaza-7-phosphaadamantane (PTA) and 4-(2-aminoethyl)morpholine were purchased from Sigma Aldrich. The complex Ru(CO)₃-(DMSO)Cl₂ (**3**)³⁵ and the ligand 3,7-diacetyl-1,3,7-triaza-5-phosphabicyclo[3.3.1]nonane (DAPTA)³³ were prepared using literature methods. Methyl 2-isocyano-2-methylbutanoate, ethyl 1-isocyanocyclopropanecarboxylate and methyl 2-isocyano-2-methylpropanoate were purchased from GalChimia, Spain.

cis,trans,cis- and cis,cis,cis-Ru(CO)₂(DMSO)₂Cl₂ (4a, 4b). [Ru(CO)₃Cl₂]₂ (0.398 g, 0.778 mmol) was dissolved in DMSO (3 mL). The reaction mixture turned orange and was stirred for 30 min at room temperature. The crude product was extracted from the DMSO solution with diethyl ether until the extracts were colourless. The ether filtrates were collected, concentrated and placed at 4 °C overnight affording an off-white solid (0.269 g; 90%). The spectroscopic data confirm the presence of both known isomers in the solid and is given here for conven-

ience.³⁵ Selected IR (KBr, cm^{-1}) 2077 (s, C=O); 2020 (s, C=O); 1132 (m, Ru-S); 1029 (m, Ru-S); 924 (m, Ru-O). ¹H NMR (CDCl_3 , 400 MHz): δ (ppm) 3.44 (s, 2H, *cis*, *trans*, *cis*-isomer), 3.43 (s, 1H), 3.17 (s, 1H), 2.88 (s, 1H), 2.85 (s, 1H, *cis*, *cis*, *cis*-isomer). ¹³C NMR (CDCl_3 , 100 MHz): δ (ppm) 185.7 (CO), 45.1 (*cis*, *trans*, *cis*-isomer), 186.1 (CO), 47.5, 42.2, 39.3, 38.9 (*cis*, *cis*, *cis*-isomer).

***cis,cis,cis*-, *cis,cis,trans*-, and *cis,mer*-Ru(CO)(DMSO)₃Cl₂ (5).** To a stirred orange solution of $[\text{Ru}(\text{CO})_3\text{Cl}_2]_2$ (0.530 g, 1.035 mmol) in DMSO (15 mL) was added toluene (15 mL). The reaction mixture was refluxed for 2 h and turned light yellow. The cooled reaction mixture was filtered at room temperature, giving a turbid suspension, which was then filtered. To the filtrate, diethyl ether was added and the solution was placed at -30°C overnight. An oily yellow residue and a white crystalline product were precipitated. From the cold filtrate, another fraction of white crystalline product with yellow contamination was obtained. This was extracted with ether, leaving a yellow powder behind and a white powder started to precipitate from the ethereal solution. After concentration and cooling, the precipitate was filtered, washed with hexane and dried *in vacuo* affording a white powder (Fraction 1). The yellow crude product was crystallised from CH_2Cl_2 -hexane at -30°C affording yellow crystals. Yield: 31%. Anal. Calcd for $\text{RuC}_7\text{H}_{18}\text{O}_4\text{S}_3\text{Cl}_2$: C, 19.36; H, 4.18; S, 22.15; Found: (Fraction 1): C, 19.40; H, 3.84; S, 22.40; Fraction 2: C, 19.83; H, 3.81; S, 22.32. Selected IR (KBr, cm^{-1}): Fraction 1: 2001 (vs, C=O); Fraction 2: 2003 (vs, C=O). ¹H NMR (CDCl_3 , 400 MHz): Both fractions contained both isomers but in different ratios: δ (ppm) 2.75 (s, 1H), 2.78 (s, 1H), 3.17 (s, 1H), 3.45 (s, 2H), 3.52 (s, 1H) assigned to the *cis*, *cis*, *cis*-isomer; 2.85 (s, 2H), 3.25 (s, 2H), 3.43 (s, 2H) assigned to the *cis*, *cis*, *trans*-isomer; 3.41 (s, 2H), 3.43 (s, 2H), 3.51 (s, 2H) assigned to the *cis*, *mer*-isomer; ¹³C NMR (CDCl_3 , 100 MHz): δ (ppm) 38.5, 39.0, 43.5, 45.3, 46.8, 50.2 assigned to the *cis*, *cis*, *cis*-isomer; 39.1, 43.7, 47.6 assigned to the *cis*, *cis*, *trans*-isomer; 42.9, 46.4, 47.4 assigned to the *cis*, *mer*-isomer. While fraction 1 has CO resonances at $\delta = 192.3$ and 191.0 ppm, no CO resonances were observed for fraction 2.

***L*-Ru(CO)₃Cl₂(H₃CSO(CH₂)₂CH(NH₂)CO₂H) (6a).** $[\text{Ru}(\text{CO})_3\text{Cl}_2]_2$ (0.918 g, 1.793 mmol) and *L*-methionine sulfoxide (0.592 g, 3.586 mmol) were suspended in acetone (100 mL), and left to react for 24 h, at room temperature. The pale yellow solution was filtered, concentrated, transferred *via* a cannula to a Schlenk tube with an excess of diethyl ether and an off-white solid was precipitated. The solid was washed with diethyl ether (2×20 mL), and dried in a vacuum (1.25 g; 83%). Anal. Calcd for $\text{RuC}_8\text{H}_{11}\text{NO}_6\text{SCl}_2$: C, 23.07; H, 2.64; N, 2.73; S, 7.57; Found: C, 22.73; H, 2.99; N, 2.95; S, 7.48. Selected IR (KBr, cm^{-1}): 2131 (s, C=O); 2055 (s, C=O); 1651 (s, C=O). ¹H NMR (MeOD, 400 MHz): δ (ppm) 4.1–3.8 (m, 1H), 3.1–2.9 (m, 2H), 2.70 (s, 3H), 2.5–2.1 (m, 2H).

***D,L*-Ru(CO)₃Cl₂(H₃CSO(CH₂)₂CH(NH₂)CO₂H) (6b).** The compound is prepared exactly as **6a** above. However, precipitation had to be induced at -30°C and the yield was considerably lower (36%). Anal. Calcd for $\text{RuC}_8\text{H}_{11}\text{NO}_6\text{SCl}_2$: C, 23.07; H,

2.64; N, 2.73; S, 7.57; Found: C, 23.17; H, 2.79; N, 3.11; S, 7.21. Selected IR (KBr, cm^{-1}): 2133 (s, C=O); 2056 (s, C=O); 1651 (s, C=O). ¹H NMR (D_2O , 400 MHz): δ (ppm) 4.06 (m, 1H), 3.09 (m, 2H), 2.76 (s, 3H), 2.39 (m, 2H).

Ru(CO)₃Cl₂(3-NC₅H₄(CH₂)₂SO₃Na) (7). $[\text{Ru}(\text{CO})_3\text{Cl}_2]_2$ (0.634 g, 1.238 mmol) and 3-NC₅H₄(CH₂)₂SO₃Na (0.518 g, 2.476 mmol) were suspended in acetone (100 mL) and left to react for 24 h, at room temperature. The solution was filtered, concentrated, transferred *via* a cannula to a Schlenk tube with an excess of diethyl ether and a pale yellow solid was precipitated. The solid was washed with diethyl ether (3×15 mL), and dried in a vacuum (0.73 g; 63%). Anal. Calcd for $\text{RuC}_{10}\text{H}_8\text{NO}_6\text{SNaCl}_2$: C, 25.82; H, 1.73; N, 3.01; S, 6.89; Found: C, 25.40; H, 1.98; N, 2.77; S, 7.12. Anal. Calc. for $\text{RuC}_{10}\text{H}_8\text{NO}_6\text{SNaCl}_2 \cdot 0.15\text{H}_2\text{O}$: C, 25.67; H, 1.79; N, 2.99; S, 6.85. Selected IR (KBr, cm^{-1}): 2137 (s, C=O); 2053 (s, C=O). ¹H NMR (D_2O , 400 MHz): δ (ppm) 8.75 (s, 1H), 8.67 (d, 1H), 8.58 (d, 1H), 8.03 (t, 1H), 3.34 (s, 4H).

Ru(CO)₃Cl₂(4-NC₅H₄(CH₂)₂SO₃Na) (8). A solution of $[\text{Ru}(\text{CO})_3\text{Cl}_2]_2$ (0.392 g, 0.765 mmol) in MeOH (20 mL) was added to a solution of the pyridine 4-NC₅H₄(CH₂)₂SO₃Na ligand (0.320 g, 1.530 mmol) in MeOH (50 mL). The colourless reaction mixture was stirred for 24 h at room temperature. The solution was filtered, concentrated and after the addition of diethyl ether a white solid was precipitated. The solid was washed with diethyl ether (2×10 mL) and dried in a vacuum (0.380 g, 53%). Anal. Calcd for $\text{RuC}_{10}\text{H}_8\text{NO}_6\text{SNaCl}_2$: C, 25.82; H, 1.73; N, 3.01; S, 6.89; Found: C, 26.10; H, 2.20; N, 3.21; S, 6.96. Anal. Calc. for $\text{RuC}_{10}\text{H}_8\text{NO}_6\text{SNaCl}_2 \cdot 0.1\text{H}_2\text{O}$: C, 25.72; H, 1.77; N, 3.00; S, 6.87. Selected IR (KBr, cm^{-1}): 2137 (s, C=O); 2053 (s, C=O). ¹H NMR (D_2O , 400 MHz): δ (ppm) 8.69 (d, 2H), 8.02 (d, 2H), 3.40 (s, 4H).

Ru(CO)₃Cl₂(PTA) (9). A solution of $[\text{Ru}(\text{CO})_3\text{Cl}_2]_2$ (0.308 g, 0.601 mmol) in MeOH (10 mL) was added to a solution of 1,3,5-triaza-7-phosphaadamantane (0.189 g, 1.203 mmol) in MeOH (10 mL), and a white precipitate was readily formed. The reaction mixture was stirred for 15 min at room temperature. The precipitate was isolated, washed with MeOH (5 mL) and dried in a vacuum (0.280 g, 56%). Anal. Calcd for $\text{N}_3\text{O}_3\text{PCl}_2\text{RuC}_9\text{H}_{12}$: C, 26.16; H, 2.93; N, 10.17; Found: C, 25.90; H, 3.30; N, 10.18. Selected IR (KBr, cm^{-1}): 2134 (w, C=O); 2060 (s, C=O); 1994 (s, C=O). ³¹P NMR (d^6 -DMSO, 162 MHz): δ (ppm) -28.84 .

Ru(CO)₃Cl₂(DAPTA) (10). A solution of $[\text{Ru}(\text{CO})_3\text{Cl}_2]_2$ (0.304 g, 0.594 mmol) in MeOH (10 mL) was added to a solution of DAPTA (0.272 g, 1.188 mmol) in MeOH (10 mL). The reaction mixture was stirred for 2 h at room temperature. The solvent was removed and the white resulting solid was washed with dichloromethane (2×10 mL) and dried in a vacuum (0.432 g, 75%). Anal. Calcd for $\text{C}_{12}\text{H}_{16}\text{Cl}_2\text{N}_3\text{O}_5\text{PRu}$: C, 29.70; H, 3.32; N, 8.66; Found: C, 29.34; H, 3.65; N, 8.47. Selected IR (KBr, cm^{-1}): 2135 (w, C=O); 2067 (s, C=O); 2001 (s, C=O); 1635 (s, C=O). ¹H NMR (D_2O , 400 MHz): δ (ppm) 5.7–3.8 (m, 8H), 3.28 (s, 2H), 2.12 (s, 6H). ³¹P NMR (CD_3OD , 162 MHz): δ (ppm) 5.87.

Ru(CO)₃Cl₂(H₃CS(CH₂)₂CH(OH)CO₂H) (11). Ligand synthesis: $[\text{H}_3\text{CS}(\text{CH}_2)_2\text{CH}(\text{OH})\text{COO}]_2\text{Ca}$ (880 mg, 2.600 mmol)

was dissolved in water (30 mL) and the solution was stirred for a couple of minutes, after which time the residue was completely dissolved. Sulfuric acid (1 M) was slowly added (2.6 mL, 1 equiv.) and the clear solution became turbid after some minutes. The solution was stirred for 90 min after which time the reaction was stopped. A white precipitate (CaSO₄) was filtered off and washed with a small amount of MeOH. The solution was dried affording a pale yellow oily residue. The residue was extracted with MeOH, leaving a small amount of a white powder behind (CaSO₄). The pale yellow filtrate was taken to dryness affording a yellow oil that was kept at -30 °C. Yield: 85%. ¹H NMR (400 MHz, CD₃OD, RT): δ 4.26 (m, 1H), 2.62 (t, 2H), 2.09 (s, 3H), 2.03 (m, 1H), 1.88 (m, 1H). ¹³C NMR (100 MHz, CD₃OD, RT): δ 177.6 (CO), 70.0, 34.8, 30.6, 15.1. IR (KBr, cm⁻¹): 1733 (s, C=O); 1437 (m); 1276 (w); 1224 (m); 1173 (m); 1096 (s); 970 (w); 799 (w); 752 (w); 656 (w); 647 (w). Complex **11** was obtained following an identical procedure to that described for **6a** and **6b**; precipitation of the complex was induced at -90 °C. Yield: 83%. ¹H NMR (400 MHz, MeOD, RT): δ 2.65 (m, 1H), 2.09 (s, 3H), 1.55–1.63 (m, 4H). IR (KBr, cm⁻¹): 2141 (s, C≡O); 2077 (s, C≡O); 2063 (s, C≡O); 1793 (s, C=O). Anal. Calcd for RuC₈H₁₀O₆SCl₂: C, 23.66; H, 2.48; S, 7.89; Found: C, 23.58; H, 2.40; S, 7.93.

Ru(CO)₃Cl₂(CNMe₂CO₂Me) (**12**). [Ru(CO)₃Cl₂]₂ (0.400 g; 0.78 mmol) was suspended and stirred in 20 mL of CHCl₃. Methyl 2-isocyano-2-methylpropanoate (3 eq.; 0.298 g) was dissolved in 10 mL of CHCl₃ and added at room temperature. After 30 min the solution was completely clear and with a yellow pale color. The reaction was continued for 5 hours. The solution was concentrated and on addition of diethyl ether a white precipitate was formed. The solid was filtered and dried in a vacuum (0.67 g, 96%). Anal. Calcd for RuC₉H₉Cl₂NO₅: %C, 28.21; H, 2.37; N, 3.66. Found: C, 27.90; H, 2.53; N, 3.60. Selected IR (KBr, cm⁻¹): 2247 (s, C≡N); 2145 (s, C≡O), 2094 (s, C≡O), 2058 (s, C≡O); 1750 (C=O). ¹H NMR (CDCl₃, 400 MHz): 3.89 (s, 3H, O-CH₃); 1.85 (s, 6H). ¹³C NMR (CDCl₃): δ (ppm) 183 (C=O); 182 (C=O); 169 (C≡N); 65 (C-(CH₃)₂); 54 (OCH₃); 27 (C-(CH₃)₂).

Note: Attempts to recrystallize the compound in a mixture of chloroform and diethyl ether, at -30 °C, gave rise to a yellow solid. The FTIR is in agreement with this compound being a dicarbonyl, but its full characterization was not pursued. Selected IR (KBr, cm⁻¹): 2230 m (C≡N), 2093 s, 2037 s (C=O), 1758 m (C=O).

Ru(CO)₃Cl₂(CNMeEtCO₂Me) (**13**). [Ru(CO)₃Cl₂]₂ (0.40 g; 0.78 mmol) was suspended in chloroform (25 mL) and treated with methyl 2-isocyano-2-methylbutanoate (0.334 g; 2.36 mmol). The yellow pale solution was stirred for 5 hours, at room temperature. The solution was reduced in volume and diethyl ether (30 mL) was added and placed at -30 °C overnight. A pale yellow solid was isolated (0.11 g; 18%). Recrystallization of the solid in a mixture of chloroform and diethyl ether, at -30 °C, gave rise to crystals. Anal. Calcd for RuC₁₀H₁₁NO₅Cl₂: C, 30.24; H, 2.79; N, 3.53; Found: C, 30.50; H, 2.98; N, 3.72. Selected IR (KBr, cm⁻¹): 2252 m (C≡N), 2149 vs, 2090 s, 2061 vs (C=O), 1753 m (C=O). ¹H NMR (CDCl₃, 400 MHz):

δ (ppm) 3.88 (s, 3H), 2.12 (m, 2H, 3H), 1.79 (s, 3H), 1.11 (t, 3H). ¹³C NMR (CDCl₃, 100 MHz): δ (ppm) 183 (C=O), 181 (C=O), 168 (C≡N), 69 (CCH₃C₂H₅), 54 (OCH₃), 33 (CCH₂CH₃), 25 (CCH₃), 9 (CH₂CH₃).

Ru(CO)₃Cl₂(CN(c-CCH₂CH₂)CO₂Et) (**14**). [Ru(CO)₃Cl₂]₂ (0.250 g; 0.49 mmol) was suspended in chloroform (20 mL) and treated with ethyl 1-isocyanocyclopropanecarboxylate (0.208 g; 1.49 mmol). The yellow pale solution was stirred for 5 hours, at room temperature. The solution was concentrated and diethyl ether (30 mL) was added, and placed at -30 °C overnight. The white solid was isolated and washed with diethyl ether (0.37 g; 96%). Anal. Calcd for RuC₁₀H₁₁NO₅Cl₂: C, 30.39; H, 2.30; N, 3.54; Found: C, 30.30; H, 2.21; N, 3.58. Selected IR (KBr, cm⁻¹): 2249 m (C≡N), 2140 vs, 2093 s, 2070 vs (C=O), 1738 m (C=O). ¹H NMR (CDCl₃, 400 MHz): δ (ppm) 4.32 (q, 2H), 1.88 (s, 4H), 1.36 (t, 3H). ¹³C NMR (CDCl₃, 100 MHz): δ (ppm) 183 (C=O), 181 (C=O), 166 (C≡N), 64 (CH₂CH₃), 63 (C(CH₂CH₂)), 21 (C(CH₂CH₂)), 14 (CH₂CH₃).

Conflict of interest

All the authors designated as affiliated with Alfama Ltd were paid by that company to perform the work described herein and have equity interests (except for G.J.L.B.).

Acknowledgements

We thank Fundação para a Ciência e Tecnologia (FCT), Portugal (PTDC/QUI-BIQ/117799/2010, PEst-C/EQB/LA0006/2013 and PEst-OE/QUI/UI0100/2013) for funding. J.D.S. and M.F.A.S. thank FCT for the award of doctoral studentships. A.M., A.C.C. and P.M.R. thank FCT for the award of postdoctoral fellowships. The National NMR Network (REDE/1517/RMN/2005) was supported by POCI 2010 (FEDER) and FCT. We also thank the ESRF for provision of synchrotron radiation facilities (beamlines ID14-1 and ID14-2).

Notes and references

- 1 A. Verma, D. J. Hirsch, C. E. Glatt, G. V. Ronnett and S. H. Snyder, *Science*, 1993, **259**, 381–384.
- 2 L. Otterbein, F. Bach, J. Alam, M. Soares, H. Lu, M. Wysk, R. Davis, R. Flavell and A. Choi, *Nat. Med.*, 2000, **6**, 422–428.
- 3 R. Buelow and J. Woo, *WO 2002/078684*, 20020401, 2002.
- 4 R. Motterlini and B. E. Mann, *WO 2002/092075*, 20020515, 2002.
- 5 W. Haas, C. C. Romão, B. Royo, A. Fernandes and I. Gonçalves, *WO 2003/066067*, 20030203, 2003.
- 6 R. Motterlini, J. Clark, R. Foresti, P. Sarathchandra, B. Mann and C. Green, *Circ. Res.*, 2002, **90**, E17–E24.

- 7 J. Clark, P. Naughton, S. Shurey, C. Green, T. Johnson, B. Mann, R. Foresti and R. Motterlini, *Circ. Res.*, 2003, **93**, E2–E8.
- 8 B. E. Mann, *Organometallics*, 2012, **31**, 5728–5735.
- 9 I. C. Winburn, K. Gunatunga, R. D. McKernan, R. J. Walker, I. A. Sammut and J. C. Harrison, *Basic Clin. Pharmacol. Toxicol.*, 2012, **111**, 31–41.
- 10 Y. Guo, A. B. Stein, W.-J. Wu, W. Tan, X. Zhu, Q.-H. Li, B. Dawn, R. Motterlini and R. Bolli, *Am. J. Physiol. Heart C*, 2004, **286**, H1649–H1653.
- 11 G. Wang, T. Hamid, R. J. Keith, G. Zhou, C. R. Partridge, X. Xiang, J. R. Kingery, R. K. Lewis, Q. Li, D. G. Rokosh, R. Ford, F. G. Spinale, D. W. Riggs, S. Srivastava, A. Bhatnagar, R. Bolli and S. D. Prabhu, *Circulation*, 2010, **121**, 1912–1925.
- 12 M. Musameh, C. Green, B. Mann, B. Fuller and R. Motterlini, *J. Heart Lung Transplant.*, 2007, **26**, 1192–1198.
- 13 B. Chen, L. Guo, C. Fan, S. Bolisetty, R. Joseph, M. M. Wright, A. Agarwal and J. F. George, *Am. J. Pathol.*, 2009, **175**, 422–429.
- 14 R. Motterlini and L. E. Otterbein, *Nat. Rev. Drug Discovery*, 2010, **9**, 728–743.
- 15 B. E. Mann, *Top. Organomet. Chem.*, 2010, **32**, 247–285.
- 16 E. A. Sher, M. Shaklai and N. Shaklai, *Adv. Biol. Chem.*, 2012, **2**, 191–197.
- 17 A. Marazioti, M. Bucci, C. Coletta, V. Vellecco, P. Baskaran, C. Szabó, G. Cirino, A. R. Marques, B. Guerreiro, A. M. L. Gonçalves, J. D. Seixas, A. Beuve, C. C. Romão and A. Papapetropoulos, *Arterioscler., Thromb., Vasc. Biol.*, 2011, **31**, 2570–2576.
- 18 A. C. Pena, N. Penacho, L. Mancio-Silva, R. Neres, J. D. Seixas, A. C. Fernandes, C. C. Romão, M. M. Mota, G. J. L. Bernardes and A. Pamplona, *Antimicrob. Agents Chemother.*, 2012, **56**, 1281–1290.
- 19 R. Cini, S. Defazio, G. Tamasi, M. Casolaro, L. Messori, A. Casini, M. Morpurgo and M. Hursthouse, *Inorg. Chem.*, 2007, **46**, 79–92.
- 20 D. Valensin, P. Anzini, E. Gaggelli, N. Gaggelli, G. Tamasi, R. Cini, C. Gabbiani, E. Michelucci, L. Messori, H. Kozlowski and G. Valensin, *Inorg. Chem.*, 2010, **49**, 4720–4722.
- 21 M. F. A. Santos, J. D. Seixas, A. C. Coelho, A. Mukhopadhyay, P. M. Reis, M. J. Romão, C. C. Romão and T. Santos-Silva, *J. Inorg. Biochem.*, 2012, **117**, 285–291.
- 22 C. C. Romão, W. A. Blättler, J. D. Seixas and G. J. L. Bernardes, *Chem. Soc. Rev.*, 2012, **41**, 3571–3583.
- 23 S. García-Gallego and G. J. L. Bernardes, *Angew. Chem., Int. Ed.*, 2014, **53**, 9712–9721.
- 24 M. Desmard, R. Foresti, D. Morin, M. Dagouassat, A. Berdeaux, E. Denamur, S. H. Crook, B. E. Mann, D. Scapens, P. Montravers, J. Boczkowski and R. Motterlini, *Antioxid. Redox Signaling*, 2012, **16**, 153–163.
- 25 S. McLean, B. E. Mann and R. K. Poole, *Anal. Biochem.*, 2012, **427**, 36–40.
- 26 T. Santos-Silva, A. Mukhopadhyay, J. D. Seixas, G. J. L. Bernardes, C. C. Romão and M. J. Romão, *J. Am. Chem. Soc.*, 2011, **133**, 1192–1195.
- 27 T. Santos-Silva, A. Mukhopadhyay, J. D. Seixas, G. J. L. Bernardes, C. C. Romão and M. J. Romão, *Curr. Med. Chem.*, 2011, **18**, 3361–3366.
- 28 P. Wang, H. Liu, Q. Zhao, Y. Chen, B. Liu, B. Zhang and Q. Zheng, *Eur. J. Med. Chem.*, 2014, **74**, 199–215.
- 29 B. W. Michel, A. R. Lippert and C. J. Chang, *J. Am. Chem. Soc.*, 2012, **134**, 15668–15671.
- 30 M. Moreno, M. Haukka and M. Kallinen, *Appl. Organomet. Chem.*, 2006, **20**, 51–69.
- 31 R. K. Hom and J. A. Katzenellenbogen, *Nucl. Med. Biol.*, 1997, **24**, 485–498.
- 32 A. R. Marques, L. Kromer, D. J. Gallo, N. Penacho, S. S. Rodrigues, J. D. Seixas, G. J. L. Bernardes, P. M. Reis, S. L. Otterbein, R. A. Ruggieri, A. S. G. Gonçalves, A. M. L. Gonçalves, M. N. D. Matos, I. Bento, L. E. Otterbein, W. A. Blättler and C. C. Romão, *Organometallics*, 2012, **31**, 5810–5822.
- 33 D. Darensbourg, C. Ortiz and J. Kamplain, *Organometallics*, 2004, **23**, 1747–1754.
- 34 J.-R. Li and X.-H. Bu, *Eur. J. Inorg. Chem.*, 2008, 27–40.
- 35 E. Alessio, B. Milani, M. Bolle, G. Mestroni, P. Faleschini, F. Todone, S. Geremia and M. Calligaris, *Inorg. Chem.*, 1995, **34**, 4722–4734.
- 36 D. Darensbourg, F. Joo, M. Kannisto, A. Katho, J. Reibenspies and D. Daigle, *Inorg. Chem.*, 1994, **33**, 200–208.
- 37 D. N. Akbayeva, L. Gonsalvi, W. Oberhauser, M. Peruzzini, F. Vizza, P. Brüggeller, A. Romerosa, G. Sava and A. Bergamo, *Chem. Commun.*, 2003, 264–265.
- 38 M. Calligaris, *Coord. Chem. Rev.*, 2004, **248**, 351–375.
- 39 I. Evans, A. Spencer and G. Wilkinson, *J. Chem. Soc., Dalton Trans.*, 1973, 204–209.
- 40 E. Alessio, G. Mestroni, G. Nardin, W. Attia, M. Calligaris, G. Sava and S. Zorzet, *Inorg. Chem.*, 1988, **27**, 4099–4106.
- 41 C. Allardyce, P. Dyson, D. Ellis and S. Heath, *Chem. Commun.*, 2001, 1396–1397.
- 42 T. Funaioli, C. Cavazza, F. Marchetti and G. Fachinetti, *Inorg. Chem.*, 1999, **38**, 3361–3368.
- 43 T. R. Johnson, B. E. Mann, I. P. Teasdale, H. Adams, R. Foresti, C. J. Green and R. Motterlini, *Dalton Trans.*, 2007, 1500–1508.
- 44 M. C. Vaney, S. Maignan, M. Ries-Kautt and A. Ducruix, *Acta Crystallogr., Sect. D: Biol. Crystallogr.*, 1996, **52**, 505–517.
- 45 U. Meier, R. Scopelliti, E. Solari and A. Merbach, *Inorg. Chem.*, 2000, **39**, 3816–3822.
- 46 M. Torrent, M. Sola and G. Frenking, *Organometallics*, 1999, **18**, 2801–2812.
- 47 S. Barrows, *Inorg. Chem.*, 2004, **43**, 8236–8238.
- 48 X. Rozanska and R. Vuilleumier, *Inorg. Chem.*, 2008, **47**, 8635–8640.
- 49 F. Zhang, L. Zhao, C. Xu and Y. Chen, *Inorg. Chem.*, 2010, **49**, 3278–3281.
- 50 N. Kuriakose, S. Kadam and K. Vanka, *Inorg. Chem.*, 2012, **51**, 377–385.

- 51 Y. Chen, F. Zhang, C. Xu, J. Gao, D. Zhai and Z. Zhao, *J. Phys. Chem. A*, 2012, **116**, 2529–2535.
- 52 H. Schulz, A. Goerling and W. Hieringer, *Inorg. Chem.*, 2013, **52**, 4786–4794.
- 53 G. Laurency, L. Helm, A. Ludi and A. Merbach, *Helv. Chim. Acta*, 1991, **74**, 1236–1238.
- 54 H. Vreman, R. Wong, T. Kadotani and D. Stevenson, *Anal. Biochem.*, 2005, **341**, 280–289.
- 55 A. B. Stein, R. Bolli, B. Dawn, S. K. Sanganalmath, Y. Zhu, O. L. Wang, Y. Guo, R. Motterlini and Y. T. Xuan, *J. Mol. Cell. Cardiol.*, 2012, **52**, 228–236.
- 56 W. Fehlhammer, S. Schrollkamp, M. Hoyer, H. Hartl and W. Beck, *Z. Anorg. Allg. Chem.*, 2005, **631**, 3025–3029.
- 57 D. Achatz, M. Lang, A. Volkl, W. Fehlhammer and W. Beck, *Z. Anorg. Allg. Chem.*, 2005, **631**, 2339–2346.
- 58 S.-I. Murahashi, T. Nakae, H. Terai and N. Komiya, *J. Am. Chem. Soc.*, 2008, **130**, 11005–11012.
- 59 D. Chatterjee, A. Mitra and R. van Eldik, *Dalton Trans.*, 2007, 943–948.
- 60 A. F. N. Tavares, M. Teixeira, C. C. Romão, J. D. Seixas, L. S. Nobre and L. M. Saraiva, *J. Biol. Chem.*, 2011, **286**, 26708–26717.
- 61 S. Werner, N. Szesni, A. Bittermann, M. J. Schneider, P. Härtel, M. Haumann and P. Wasserscheid, *Appl. Catal., A*, 2010, **377**, 70–75.
- 62 H. Ishida, K. Tanaka, M. Morimoto and T. Tanaka, *Organometallics*, 1986, **5**, 724–730.
- 63 H. Tanaka, H. Nagao, S. Peng and K. Tanaka, *Organometallics*, 1992, **11**, 1450–1451.
- 64 H. Tanaka, B. Tzeng, H. Nagao, S. Peng and K. Tanaka, *Organometallics*, 1992, **11**, 3171–3172.
- 65 G. N. Murshudov, A. A. Vagin and E. J. Dodson, *Acta Crystallogr., Sect. D: Biol. Crystallogr.*, 1997, **53**, 240–255.
- 66 P. Emsley and K. Cowtan, *Acta Crystallogr., Sect. D: Biol. Crystallogr.*, 2004, **60**, 2126–2132.
- 67 R. P. Joosten, K. Joosten, G. N. Murshudov and A. Perrakis, *Acta Crystallogr., Sect. D: Biol. Crystallogr.*, 2012, **68**, 484–496.
- 68 M. J. Frisch, G. W. Trucks, H. B. Schlegel, G. E. Scuseria, M. A. Robb, J. R. Cheeseman, G. Scalmani, V. Barone, B. Mennucci, G. A. Petersson, H. Nakatsuji, M. Caricato, X. Li, H. P. Hratchian, A. F. Izmaylov, J. Bloino, G. Zheng, J. L. Sonnenberg, M. Hada, M. Ehara, K. Toyota, R. Fukuda, J. Hasegawa, M. Ishida, T. Nakajima, Y. Honda, O. Kitao, H. Nakai, T. Vreven, J. A. Montgomery, Jr., J. E. Peralta, F. Ogliaro, M. Bearpark, J. J. Heyd, E. Brothers, K. N. Kudin, V. N. Staroverov, R. Kobayashi, J. Normand, K. Raghavachari, A. Rendell, J. C. Burant, S. S. Iyengar, J. Tomasi, M. Cossi, N. Rega, J. M. Millam, M. Klene, J. E. Knox, J. B. Cross, V. Bakken, C. Adamo, J. Jaramillo, R. Gomperts, R. E. Stratmann, O. Yazyev, A. J. Austin, R. Cammi, C. Pomelli, J. W. Ochterski, R. L. Martin, K. Morokuma, V. G. Zakrzewski, G. A. Voth, P. Salvador, J. J. Dannenberg, S. Dapprich, A. D. Daniels, O. Farkas, J. B. Foresman, J. V. Ortiz, J. Cioslowski and D. J. Fox, *GAUSSIAN 09 (Revision A.01)*, Gaussian, Inc., Wallingford CT, 2009.
- 69 W. J. Hehre, L. Radom, P. von Ragué Schleyer and J. A. Pople, *Ab Initio Molecular Orbital Theory*, John Wiley & Sons, New York, 1986.
- 70 R. G. Parr and W. Yang, *Density Functional Theory of Atoms and Molecules*, Oxford University Press, New York, 1989.
- 71 J. P. Perdew, K. Burke and M. Ernzerhof, *Phys. Rev. Lett.*, 1997, **78**, 1396–1396.
- 72 J. P. Perdew, *Phys. Rev. B: Condens. Matter*, 1986, **33**, 8822–8824.
- 73 U. Haussermann, M. Dolg, H. Stoll, H. Preuss, P. Schwerdtfeger and R. M. Pitzer, *Mol. Phys.*, 1993, **78**, 1211–1224.
- 74 W. Kuchle, M. Dolg, H. Stoll and H. Preuss, *J. Chem. Phys.*, 1994, **100**, 7535–7542.
- 75 T. Leininger, A. Nicklass, H. Stoll, M. Dolg and P. Schwerdtfeger, *J. Chem. Phys.*, 1996, **105**, 1052–1059.
- 76 A. W. Ehlers, M. Bohme, S. Dapprich, A. Gobbi, A. Hollwarth, V. Jonas, K. F. Kohler, R. Stegmann, A. Veldkamp and G. Frenking, *Chem. Phys. Lett.*, 1993, **208**, 111–114.
- 77 R. Ditchfie, W. J. Hehre and J. A. Pople, *J. Chem. Phys.*, 1971, **54**, 724–728.
- 78 W. J. Hehre, R. Ditchfield and J. A. Pople, *J. Chem. Phys.*, 1972, **56**, 2257–2261.
- 79 P. C. Harihara and J. A. Pople, *Mol. Phys.*, 1974, **27**, 209–214.
- 80 P. C. Harihara and J. A. Pople, *Theor. Chim. Acta*, 1973, **28**, 213–222.
- 81 E. Cancès, B. Mennucci and J. Tomasi, *J. Chem. Phys.*, 1997, **107**, 3032–3041.
- 82 M. Cossi, V. Barone, B. Mennucci and J. Tomasi, *Chem. Phys. Lett.*, 1998, **286**, 253–260.
- 83 B. Mennucci and J. Tomasi, *J. Chem. Phys.*, 1997, **106**, 5151–5158.
- 84 J. Tomasi, B. Mennucci and R. Cammi, *Chem. Rev.*, 2005, **105**, 2999–3093.
- 85 A. V. Marenich, C. J. Cramer and D. G. Truhlar, *J. Phys. Chem. B*, 2009, **113**, 6378–6396.
- 86 C. Y. Peng, P. Y. Ayala, H. B. Schlegel and M. J. Frisch, *J. Comput. Chem.*, 1996, **17**, 49–56.
- 87 C. Peng and H. B. Schlegel, *Isr. J. Chem.*, 1993, **33**, 449–454.